Doctoral Dissertation

Design and Development of an Autonomous Robotic Platform for Detecting, Monitoring and Tracking of Oil Spill on The Sea Surface

Swarn Singh Rathour

July 2016

Graduate School of Engineering,
Osaka University

The Dissertation Committee for Swarn Singh Rathour Certifies that this is the approved version of the following dissertation:

Design and Development of an Autonomous Robotic Platform for Detecting, Monitoring and Tracking of Oil Spill on The Sea Surface

Committee:

Prof. Kazuhiko Hasegawa

Prof. Yasuyuki Toda

Associate Professor Hiroyoshi Suzuki

Abstract

In this study, development of an autonomous robotic platform for oil spill tracking on the sea surface has been carried out. After the 2010 Deepwater Horizon accident, environmental regulations shifted to a more goal-oriented approach that required risk management plans for controlling site-specific risks. With the aim of aiding mitigation efforts, in mapping and simulating the transport of the discharged hydrocarbon this paper proposes an autonomous surface vehicle (ASV) equipped with an laser fluorescence oil detecting sensor, propelled by wind and water currents for the long-term monitoring of spilled oil on the ocean surface. The main objective of our tracking and predicting system is to allow an ASV to automatically follow a drifting oil slick and to continuously return positioning and hydrographic data to the operation base. An ASV equipped with an oil detection sensor can get closer to the oil–water interface to detect oil with greater accuracy and can continuously track the spilled oil. Such a technology, coupled with satellite and other forms of data, would facilitate the coordination of recovery operations because the data collected would better inform oil-drifting simulations, thus making it possible to predict precisely where the oil spill will travel. ASVs have the advantage of being able to track oil slicks during night when aerial surveillance of the sea surface and oil spill is impossible, thus providing a mechanism for the continuous and accurate geolocation of oil slicks.

Minor differences in the winds and water currents can cause the oil slick to become patchy. To deal with such possibility of weathering which can lead to the break-up of the oil slick into multiple clusters around the ASV named SOTAB-II, this paper makes a unique contribution to the literature in proposing a cluster-based decision-making

algorithm for sailing the SOTAB-II based on a complete scanning history of the area surrounding the vehicle by the oil detection sensor. A Gaussian-based oil cluster filtering algorithm is introduced to identify the largest oil slick patch.

The highly nonlinear dynamic model of sailboats, due to complex hull aero- and hydrodynamic models, combined with various appendages (e.g., sail, keel, and rudder), is not always suitable for optimal control of sailing vessels. The use of wind and water current for propulsion of the SOTAB-II poses a significant limitation, as the vessels lose its propulsive force from the environment as it enter “no-go-zones” (i.e., in the direction from which the wind is coming). To deal with such situation, the physical constraints of the SOTAB-II have been taken in account to allow for the computation of feasible maneuvering headings for sailing to avoid sailing upwind (i.e., in the direction from which the wind is coming).

Finally, using neoprene sheets to simulate oil spills, field test experiments are described to validate the operation of the SOTAB-II with respect to oil spill tracking using a guidance, navigation, and control system based on onboard sensor data for tracking the simulated oil spill. Three set of experiments were carried out, firstly free drifting experiments were performed to characterize the drifting behavior of the SOTAB-II with respect to wind and water current. Subsequent velocity control experiments were conducted on SOTAB-II to prove the effectiveness of sail and rudder in controlling the speed of SOTAB-II within the desired range and controlling the heading direction within the desired limits. Finally, experiment were carried out to validate the control algorithm designed for keeping SOTAB-II with the largest cluster of simulated oil spill, and the effectiveness of the control algorithm in bringing back SOTAB-II within the simulated oil spill in case if it loses the track of oil spill.

Acknowledgement

Foremost, I would like to express my sincere gratitude and thanks to my advisor Prof. Naomi Kato for accepting me as a graduate student in the Department of Naval Architecture and Ocean Engineering, Osaka University. I am also grateful to him for his continuous support of my PhD study and related research, for his patience, motivation, enthusiasm and immense knowledge. I have been trained to become a true researcher from identifying research and writing research proposals, to executing research ideas, organizing experiments, carrying out simulation, to writing concise papers and time management during my doctoral candidate life. Without his guidance and support, this dissertation would not have been completed.

Beside my advisor, I would like to thank the rest of my thesis committee: Prof. Kazuhiko Hasegawa, Prof. Yasuyuki Toda and Associate Prof. Hiroyoshi Suzuki, for their encouragement, insightful comments, and hard questions.

My sincere thanks also goes to Associate Prof. Hiroyoshi Suzuki for becoming my official guide after the retirement of Prof. Naomi Kato. I am thankful for his guidance and support in carrying out the experiment as well as in official procedures.

I am also grateful to Assistant Professor Hidetaka Senga for his guidance and help in conducting the pond and sea experiment. He always provided very insightful advice and comments.

I received help during experiment and analysis from many students of Kato laboratory, namely Mr. T. Akamatsu, Mr. N. Tanabae, Ms. Y. Hirai, Ms. Yen Chao, Ms. Okazaki and all other lab members for their support and help. I am grateful for their help.

I acknowledge Japan Ministry of higher Education, Culture, Sports, Science and Technology (MEXT) for providing me with the opportunity to pursue graduate studies in Japan and for the generous financial support throughout my study.

There are several others whom I would like to thank collectively for the sleepless nights we were working together before deadlines, and for all the fun we have had in the last three and half years. To those who feel missed out in this listing I owe my sincere apologies.

Finally, and most importantly, I am indebted to the love and support that I have received from my family members. In special, I am thankful to my parents who made several sacrifices to ensure that I could pursue my dream of furthering the education abroad to PhD. Deepest gratitude is given to my mother for her immense emotional support and constant encouragement.

Nomenclature

$\boldsymbol{V}$	SOTAB-II absolute speed
α	SOTAB-II absolute drift direction
W_a, W_r	Absolute & Relative wind speed respectively
β	Absolute wind direction
γ	Relative Wind Direction
CW_a, CW_{ar}	Absolute & Relative water current speed (surface current)
ζ	Relative water current direction
ψ	Surface Water current vector and wind vector resultant direction (absolute)
W_{a10}	Absolute wind speed at a height of 10m from sea surface
θ	SOTAB-II absolute Azimuth
TD,TD'	Target Heading, Modified Target heading
TV, TV'	Target speed, Modified Target speed
e	Relative Heading Error
P_i	Oil Sensor data set
m_i	Length of largest subarray of detected points in i^{th} sensor data set
k_i	Total number of largest subarray of detected points in i^{th} sensor data set
c_{ik}	Center of the k^{th} subarray having m_i detected points in i^{th} sensor data set

sum_{ik} k^{th} Product sum of the Gaussian function and i^{th} time history of sensor data set

$p(x_{oi}, y_{oi})$, Detected oil slick absolute position

$p(x_{si}, y_{si})$ SOTAB-II absolute position

$p(x_{oei}, y_{oei})$ Estimated oil slick position

$\emptyset$ Bearing of the estimated oil slick absolute Position from SOTAB-II absolute position

K_p, K_i, K_d PID parameters

δ Rudder Control Command

g Scaling Parameter

$m_x\ m_y\ m_z$ Hydrodynamic added mass

$C_l\ C_d$ Sail Lift and Drag Coefficient

$l\ , d$ Sail Lift and Drag forces

X_E, Y_E, N_E External forces acting on SOTAB-II hull

Table of Contents

List of Figures

LIST OF TABLES

1 Introduction

At one point in time, an oil spill accident would make the news headlines. Most people have some means of finding out about major oil spill accidents, such as the 1991 Gulf War oil spill or the 2010 Deepwater Horizon oil spill. Small and medium sized oil spills, however, often go undiscovered and unreported. Oil spill can be accidental or intentional, functional discharges and spills of oil from ships, usually tankers, offshore platforms and pipelines, and these are the most pronounced and recognizable cause of oil pollution of the marine environment. According to statistics provided by the International Tanker Owners Pollution Federation ([ITOPF] 2015), from 2000 to 2009, a total amount of 213,000 tons of oil was discharged into the sea. Preventive measures such as double hull tankers, secondary containment, and modern drilling and blowout prevention techniques significantly reduced the likelihood of an oil spill due to an accident or blowout. However, the Deepwater Horizon incident in the Gulf of Mexico (GoM) in 2010 showed, if it does occur the impacts from such an incident can be significant. No safety measure can 100% reduce the risk of an accident. After the 2010 Deepwater Horizon accident, environmental regulations shifted to a more goal-oriented approach that required risk management plans for controlling site-specific risks.

1.1 Oil Spill Disaster

The impact of these spills, however, depends upon the volume and the type of oil spilled, the ambient conditions, and the sensitivity of the affected marine ecosystem and its inhabitants to the oil. These disasters can result in significant damage to the ocean environment and regional economies. Moreover, in high volume, residual spilled oil

washing up along the coast can cause substantial long-term damage to the environment (Fingas and Charles 2001). Recovery from such damage is fraught with difficulty. After spilling into the ocean, oil tends to spread to form a slick of varying thickness depending on the viscosity of the spilled oil. In addition, minor differences in the winds and water currents can cause the oil slick to become patchy. Oil weathering and transport is generally governed by the thickness and area of the oil slick. In the presence of wind and water currents, the velocity vector of a drifting oil spill is the product of 2–5% of the wind velocity vector along the wind direction at a height of 10 m from the sea surface and the water current velocity vector (Fingas and Charles 2001). The average cost of oil spill cleanup worldwide varies from $20-$200 per liter depending on the type of the oil and where it is spilled. Ocean coast and shorelines cleaning is most expensive. Over the past several decades, a concerted scientific effort has been made to estimate the drift and spread of spilled oil on the ocean surface. Timely spill detection, real-time in situ oceanographic data, and knowledge of the oil slick's location are fundamental to reducing the environmental impact of an oil spill.

1.2 Surface Oil Spill Trajectory and Spread Estimation Methods

Oil spill sensing and drift estimation has emerged as a major component of oil spill contingency plans for the support of response decision-making, surveillance, and oil spill warning systems. With the aim of aiding mitigation efforts, in mapping and simulating the transport of the discharged hydrocarbon scientists from the operational response agencies, the academic community, and the private sector employed various possible

technologies available for oil spill detection technologies and ocean-observing and modeling resources in forecasting and monitoring of oil spill in real time. Numerous types of instruments and sensors were deployed and various numerical models were developed and applied in forecasting the transport of surface oil in the ocean environment (Reed et. al., 1999). This section briefs the pros and cons of the till date available technology for oil spill detection technologies.

1.2.1 Surface oil Spill Mapping

Airborne or space born sensors play an important role in oil spill response efforts (Jensen et al. 2008). However, still photography or video photography remains one of the most commonly practiced means of oil spill surveillance. Nevertheless, it must be remarked that oil shows no distinguishing spectral characteristics in the visible spectrum (Fingas and Brown 2007); therefore, making sense of the information from visual surveillance sensors depends more upon the expertise of the user than the discriminating ability of these optical sensors. The X-band radar detection method can be used by a vessel for oil spill detection and tracking, however, the accuracy and efficiency of X-band radar detection in either very calm or extreme wave conditions is questionable due to the capillary wave-dampening effect (Fingas and Charles 2001). Radar and aircraft are also expensive to deploy for long duration surveillance. Moreover, one of the inherent weaknesses of most sensor systems is their inability to spot oil on beaches and among weeds or debris, and to detect oil under certain lighting conditions (Fingas and Brown 2007). Lack of positive discrimination between oil and some backgrounds reduces the forensic value of these sensor systems. Notwithstanding, laser fluorosensors, with their own source of excitation, can be employed round the clock. Compact fluorescence lidar

systems (Yamagishi et al. 2000), using charge-coupled device (CCD) cameras for imaging, are used to detect the fluorescence of substances excited by laser. This equipment can be helicopter-mounted to provide images of spilled oil spreading and its classification, even in the dark. However, the remote surveillance of oceanography data via satellites and aircraft is restricted due to their temporal and geographical limitations/coverage. Helicopters, for example, cannot continuously track spilled oil because of their limited range and endurance, and the need to be mindful of the safety of the crew.

1.2.2 Drift Buoys

SAR and high-resolution visible/near-infrared-range multi spectral satellite imagery requires variety of ancillary data for prediction of surface oil slick. Ancillary data set includes ocean surface currents, winds, natural oil seeps and in situ oil observation data set. Drift buoys have traditionally been employed to track spilled oil (Goodman et al. 1995) and for logging the oceanographic data (Ocean Current). Oceanographic data and slick drift information available from these robotic platforms provides valuable information for informing oil spill monitoring and response activities. Using woodchips and cottonseed to simulate oil spills, Goodman R (1995) carried out a series of experiment in the Gulf of Mexico during March 1994 to review the efficacy of tracking buoys for oil spill response and planning. Significant differences were observed in the trajectory of the tracking buoys and simulated oil spills. Discus-shaped buoys were found to move out of the woodchip area within a few hours after deployment, while agrosphere-like buoys were found to consistently move in a manner unlike that of the woodchips. The Orion and Novatech buoys were quite effective in following oil slicks under test conditions (Fingas 2011). The hull design of these drift buoys is inspired by oceanographic buoys (i.e.,

cylindrical or spherical shapes). However, the oceanographic buoys proved to be ineffective for oil spill tracking, because the interaction of the oceanographic buoy with winds is quite different than that of oil slicks (Fingas 2011; Goodman et al. 1995).

1.2.3 Surface Oil spill trajectory Models

A significant number of studies and numerical models have been reported on predicting the movement of oil spills, including advection, spreading, dispersion and evaporation (Fay JA 1969; Fay JA 1971; Mackay & Leinonen 1977; Fingas 1999; Reed et al. 1999; Fingas 2011). These numerical models are relatively complex, requiring exact information on the environmental conditions such as winds, currents, waves, turbulence, salinity and temperature for the accurate prediction of movement of oil slicks. However, the model's accuracy is still the subject of further research as pointed out by Mariano et al. (2011). Comparative studies of oil drift trajectories calculated using the Lagrangian oil drift model and trajectory of surface drifters—using Isphere oil spill and current tracking buoys—have produced conflicting results (Ivichev et al. 2012). The estimation of oil spill trend and spread using oil drift models depends on the accuracy of real-time in-situ oceanographic data, such as ocean surface currents, the wind field, the position of the oil spill, and the scatter of the oil spillage. Hence, the real-time long-term monitoring of the drifting behavior of spilled oil on the sea surface is crucial for controlling the adverse impact of oil spills on coastal environments (Takagi et al. 2012; Tsutsukawa et al. 2012).

1.2.4 Spilled oil Tracking Autonomous Buoy

Thin oil slicks, or in cases where the oil slick is not clearly visible, require multi-sensor fusion for oil spill detection. To overcome the limitations posed by drift buoys

and in search of an alternative method for vehicles with high maneuverability at low speed, and high agility, Kato Laboratory, Dept. of Naval Architecture and Ocean Engineering has been engaged in developing “SPILLED OIL TRACKING AUTONOMOUS BUOY” (Senga, et al., 2012, 2013). Osaka University developed a Spilled Oil Tracking Autonomous Buoy (SOTAB), with descending and ascending procedures to guide itself to spilled oil, equipped with an oil detecting sensor (i.e., senses the viscosity of water around the SOTAB), and a CCD camera (Kato et al. 2010; Yoshie et al. 2009). Although SOTAB has been shown to successfully detect and autonomously track artificial oil (i.e., neoprene gum sheets) on the ocean surface utilizing a non-contact sensor (i.e., CCD camera), there have been instances of tracking failure due to sea conditions (Yoshie et al. 2009). A second prototype, SOTAB-II, was developed with a controllable sail to exploit ambient wind conditions for tracking the spilled oil and subjected to proof-of-concept testing at sea (Senga et al. 2012, 2009). By controlling the size and direction of the sail as circumstances change, SOTAB-II can drift autonomously along with the spilled oil. SOTAB-II was developed with a cylindrical body to facilitate reactions to changes in the direction of the drifting oil slick. Experimental results showed that while sail control was achieved, the drift speed of SOTAB-II was unable to match the target drifting speed (i.e., resultant speed of 3% wind speed and water current). Consequently, a yacht-shaped SOTAB-II model was proposed in order to reduce drag coefficient in water (Kato et al. 2012; Senga et al. 2013).

1.3 Concept of SOTAB-II

Autonomous surface vehicle (ASVs) and autonomous underwater vehicles (AUVs) have subsequently emerged as the preferred alternative for the in situ measurement of

oceanography data. Real-time monitoring of surface oil spill spread and drift is achievable using an oil sensor-equipped ASV. Such real-time monitoring is impractical with moored or drift buoys because of their lack of controllability and self-deployability. An autonomous sea surface vehicle using wind and surface water current energy for propulsion is a feasible long-term ocean monitoring option (Alves and Cruz 2008; Cruz and Alves 2008; Rynne and Ellenrieder 2009). Long-range oceanography observation or sea surveillance by ASV would lead to spatial and temporal sea surface measurements of a higher resolution would ordinarily be possible using ocean surface measurements obtained via oceanography buoys, floats or manned expedition and satellite observations (Rynne & Ellenrieder, 2009). Hence, the use of ASV can lead to synergistic measurement from space, air, and sea surface, which provide a higher-resolution insight into weather and other oceanography-related forecast.

The main objective of our tracking and predicting system is to allow an ASV to automatically follow a drifting oil slick and to continuously return positioning and hydrographic data to the operation base. An ASV equipped with an oil detection sensor can get closer to the oil–water interface to detect oil with greater accuracy and can continuously track the spilled oil. Such a technology, coupled with satellite and other forms of data, would facilitate the coordination of recovery operations because the data collected would better inform oil-drifting simulations, thus making it possible to predict precisely where the oil spill will travel. ASVs have the advantage of being able to track oil slicks during night when aerial surveillance of the sea surface and oil spill is impossible, thus providing a mechanism for the continuous and accurate geo-localization of oil slicks (Figure 1.1).

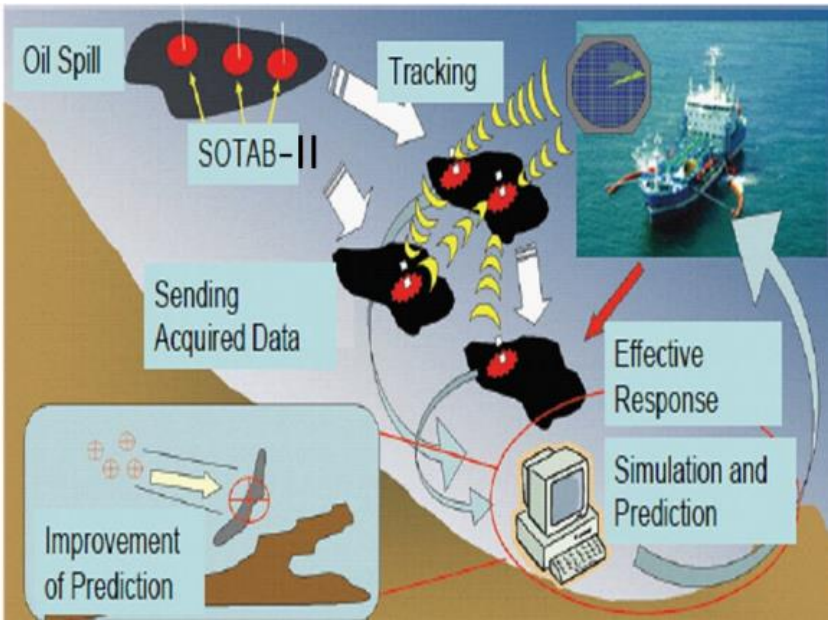

Figure 1.1 Concept of SOTAB-II

1.4 Main Contributions

- Design of a new ASV named SOTAB-II, including embedded systems, and controller for autonomous oil spill tracking.
- A decision making algorithm for guidance of SOTAB-II using point oil detection sensor with limited range.
- A cluster-based decision-making algorithm for sailing the SOTAB-II based on a complete scanning history of the area surrounding the vehicle by the oil detection sensor.
- A Gaussian-based oil cluster filtering algorithm to identify the largest oil slick patch.
- Weather routing algorithm for optimal navigation of SOTAB-II.
- The experimental outcomes of the decision making and control algorithm designed for guidance and navigation of SOTAB-II.

1.5 Outline of the Thesis

This research addresses the problem of autonomous oil spill tracking in open waters to offer high-accuracy predictions of oil slick drifting to inform the deployment of the oil collecting equipment along the ocean coast before oil drifts ashore. Chapter 2, delineates the design of a new ASV, SOTAB-II, including embedded system, actuators and the sensors used in SOTAB-II and the software module. Chapter 3, describes the prediction and derivation of the hydrodynamic parameter of the SOTAB-II hull used for model parameter identification and controller design, for the development of steering and maneuvering model of SOTAB-II. Chapter 4, deals with the water current sensor and the oil sensor calibration. It delineates the experimental setup for calibrating the oil sensor and the water current sensor. Chapter 5, delineates the decision algorithm for oil spill monitoring. A generalized clustering algorithm is introduced to deduce target heading for the ASV. Further for guidance and control of the ASV, a Gaussian based cluster filtering approach is proposed. The cluster filtering algorithm can easily be modified to filter out newborn slicks due to weathering and breaking-up of oil slicks. This could be exploited to encircle the oil spill using multiple SOTAB-II, thus providing real-time oil slick spread data. Chapter 6, briefs the weather routing algorithm for navigation of SOTAB-II taking note of physical constraints of SOTAB-II. Chapter 7 and 8 discuss the experimental outcomes of the decision making and control algorithm designed for guidance and navigation of SOTAB-II for tracking of simulated oil slick. Neoprene sheets are used for the simulated oil spill. Finally chapter 9 concludes the thesis results and brief the output of the control algorithm.

2 Design of SOTAB-II

2.1 Proposed ASV for Oil Spill Tracking in Open Waters

SOTAB-II is a flexible robotic platform, capable of carrying payloads and sensors equipment, and of storing this data onboard. SOTAB-II, an autonomous sailboat (Figure 2.1), is a small unmanned mono hull capable of fully autonomous navigation using global positioning system (GPS) data and attitude sensors based on the desired trajectory generated by its onboard guidance, navigation, and control (GNC) system. It has been designed and developed by Osaka University's Kato laboratory since 2010. A previous study (Senga et al. 2013) dealt with an earlier version of SOTAB-II. Sea experiments were conducted using the early cylindrical hull SOTAB-II at Osaka Bay, about 7 km from Awaji Island in Japan (December 21 to December 23, 2011); and lake experiments were conducted at Lake Biwa (September 29 to September 31, 2011). Three millimeter thick neoprene rubber sheets were used to simulate the oil spill. The experimental results showed that while sail control was achieved, the buoy drifting velocity was unable to match drifting speed of the target. From this experiment, it was concluded that SOTAB-II needed a larger sail to generate the required force and that the hull shape needed to be redesigned because the drag force created by the cylindrical shape of the hull was excessive, thus making auxiliary propulsion for catching up with the oil spill difficult to achieve.

Since the first SOTAB-II prototype (Senga et al. 2013), SOTAB-II has undergone two major design changes: One is the shape hull, and the other is the shape and size of the sail, keel and brake board; the reasons for these changes will be described in the design section below.

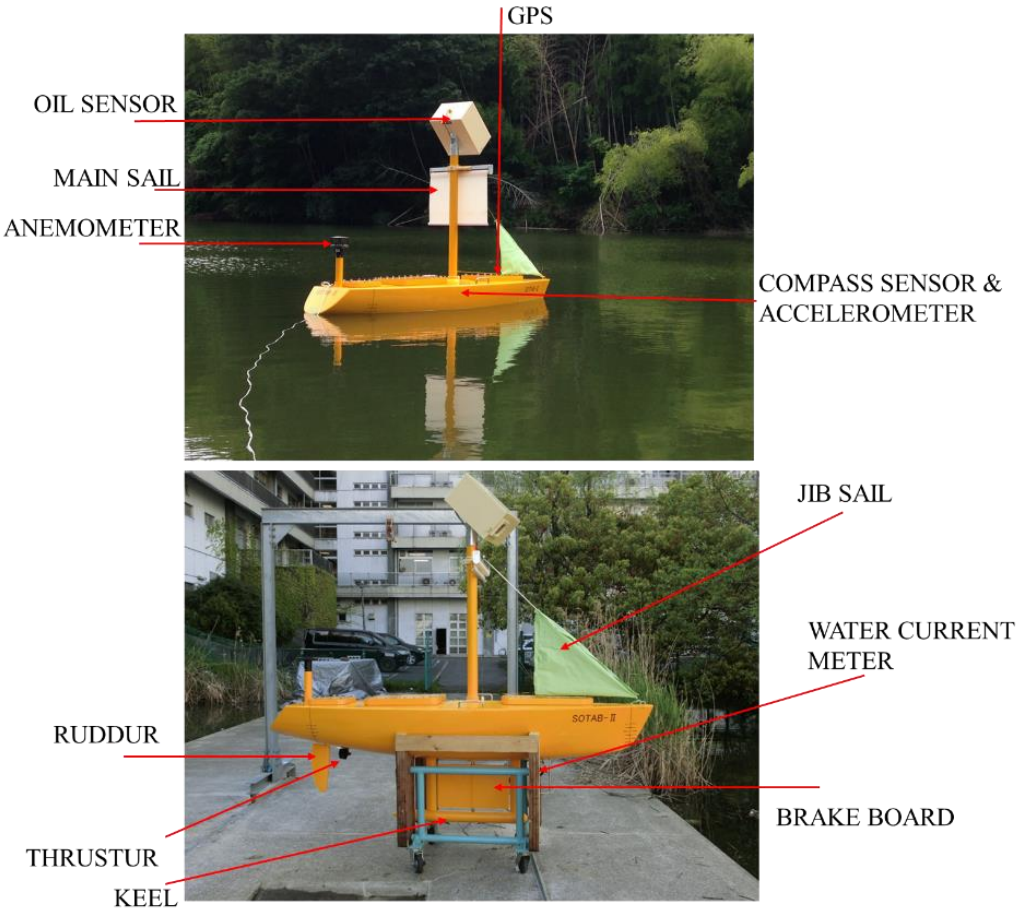

Figure 2.1 SOTAB-II prototype

2.1.1 Hull Design

A new yachted-shape SOTAB-II was designed to overcome these problems (Figure 2.1). This new SOTAB-II is a flexible robotic platform, capable of carrying payloads and sensors equipment, and of storing this data onboard. The KIT34 sailing yacht hull form, designed by Kanazawa Institute of Technology, was chosen for the new SOTAB-II hull design (Masuyama et al. 1993) due to its wider beam and larger displacement as compared to other sailing yachts of similar hull dimensions. The KIT34 hull form possesses the space requirements necessary for batteries, motors, data acquisition, and control electronics. Initially, the hull size of SOTAB-II was intended to be one fifth the size of

the KIT34 hull (Senga et al. 2013); however, the incorporation of the oil sensor (Figure 2.1), mounted at an altitude of 1.6 m above the deck and weighing approximately 10 kg with all fittings, raised SOTAB-II's center of gravity and reduced the metacentric height (GM). The quarter-sized hull was subsequently settled upon. At $\frac{1}{4}$ the original hull size, the SOTAB-II hull is a scaled-down version of the KIT34 (Rathour et al. 2014). The righting lever was found to be 147.6 mm, with a draft of 146 mm from the hull bottom, and the vanishing point of stability was found to be 125°. The main hull dimensions are indicated in Table 2-1.

Table 2-1 Physical dimensions of SOTAB-II

Total length (LOA)	2.64 m
Maximum width (Beam)	0.76 m
Draft	0.61 m
Mast height	1.60 m
Displacement	1470 N
Keel position from hull bottom	0.40 m
Keel weight	294 N

2.1.2 Mainsail & Jib Sail

SOTAB-II is fitted with two sails: jib sail and mainsail. The jib sail acts as a passive actuator to keep SOTAB-II aligned with the wind. The mainsail captures the wind to provide SOTAB-II with propulsion and modifies its speed by changing the length of the mainsail. The mainsail has only one point of freedom, thus alternating between furling

and unfurling. The proportions of the mainsail (0.75 m × 0.75 m) were designed using a computational fluid dynamics (CFD) simulation. In general, the drifting speed of an oil slick is approximately 3.0% of wind speed along the direction of the wind at a height of 10 m from the sea surface (Unoki 1993). SOTAB-II has been designed to have similar interaction with the waves and surface water currents current as that of an oil slick, hence the core objective of the mainsail is to propel SOTAB-II at a speed consistent with the wind speed affecting the oil spill. The CFD simulations demonstrated that the thrust force provided by the fully unfurled mainsail was greater than the resisting force where the drift velocity of the spilled oil is within 2%–4% of that contributed by the wind velocity. Therefore, the mainsail can provide SOTAB-II with enough thrust until the oil slick, under the condition that the drift velocity of the vehicle is caused by wind, is within 2%–4% of the wind speed (Rathour et al. 2015a).

2.1.3 Keel Design

As mentioned above, the inclusion of the oil sensor degraded the dynamic stability of SOTAB-II. Therefore, in order to increase stability and prevent the robot from capsizing in rough weather, SOTAB-II was fitted with a 0.4 m keel and a 30 kg ballast bulb, which is 80 mm deeper and 30 kg heavier that what was previously calculated (Senga et al. 2013). Taking down the keel lowers the center of gravitation of the sailboat, which makes SOTAB-II not only more stable, but also faster because less driving power is consumed when SOTAB-II remains upright.

2.1.4 Brake Board

The other major alteration made to the original design was the addition of a brake board (i.e., a flat plate) to balance the aerodynamic forces acting along the upper piece of

the body over the water surface via the hydrodynamic forces acting along the lower section of the body under the water surface. Thus, the brake (i.e., flat plate) can be used to increase roll stability as well as to gain higher speed by keeping the brake in the off position (i.e., longitudinal position). Consequently, a rectangular board, 0.50 m in width and 0.30m in height, was used for this purpose.

2.1.5 Rudder

Unlike the former design of SOTAB II, the direction of the sail in the new model is fixed. For manoeuvre control, SOTAB-II is equipped with a single rudder system, the rudder actuators assembled inside the hull are well sealed and protected against water. The rudder of the new SOTAB II is also controlled by a motor with a movable angle from -90 to 90°, while the effective operating angle is between +35 and -35°.

2.2 Hardware Description

2.2.1 Power Supply

SOTAB-II uses two 12 V lead acid batteries to power the onboard hardware. It also has one DC–DC converter for 12 V and 24 V DC output supply to meet the requirements of the sensor. For powering the onboard computer, SOTAB-II uses a DC–DC converter with a 5 V output. The oil sensor runs on AC power, hence it has a DC–AC convertor.

2.2.2 On-Board Computer

The hardware components comprising the GNC are located in the center of the hull. The main computer and various peripheral devices, such as serial–USB interfacing hardware, voltage regulator, DC–AC converter, and the wireless LAN hub, are housed in a sealed plastic fiber box. The main information-processing system for the management

of data capture and autonomous control the SOTAB-II hull is an ADVANTEC ARK-1120L, a 1.66 GHz device with 2GB RAM, and 256 GB of compact memory (Figure 4.3 (A)).

2.2.3 Actuators

For actuation of SOTAB-II, rudder angle and mainsail length are trimmed by GNC, the rudder is actuated by a servo motor (CM1-17L30C Cool Muscle with inboard motor controller and encoder) equipped with gear drive. The furling and unfurling of the mainsail is performed by a spring loaded tendon drive powered by a CM1-17L30C Cool Muscle with inboard motor controller and encoder. One end of the mainsail is fixed to the mast with a fixture mounting by spring. The brake board is driven by a worm and wheel gear drive, which is powered by a servo motor (CM1-23L20C Cool Muscle with inboard motor controller and encoder). The oil sensor shaft is also powered by a servo motor (CM1-17L30C Cool Muscle with inboard motor controller and encoder). A belt drive was used as a power transmission mechanism between the oil sensor shaft and the motor shaft.

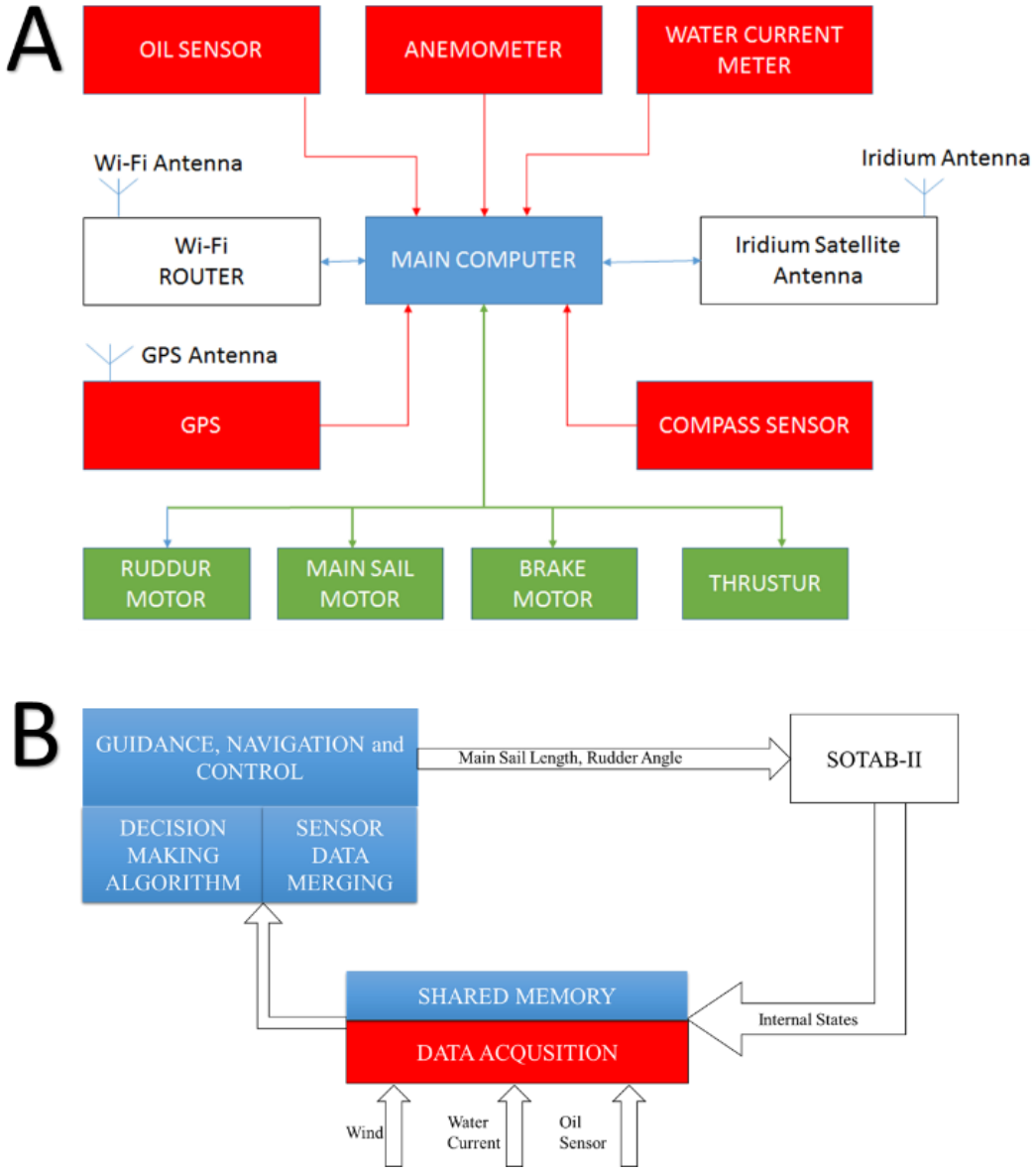

Figure 2.2 Architecture of SOTAB-II (A) Hardware architecture; (B) Software architecture

2.3 Sensors

An overview of the hardware and software architecture is illustrated in Figure 4.2 and described in Figure 4.3 (A & B). SOTAB-II uses a number of sensors for its localization and navigational purpose.

2.3.1 Guidance & Navigational Sensors

- ***Oil Sensor:*** SOTAB-II uses a Slick Sleuth SS300 as an oil sensor. The Slick Sleuth SS300 is an optical sensor that can detect micron level amounts of oil in real time from a distance of 1–5 m above the water surface. The Slick Sleuth SS300 comes with a user-selectable detection setting, enabling the user to define the detection threshold and detection period (i.e., sampling interval/frequency), from 0.5 s to 90 min.
- ***GPS:*** A Hemisphere A325™ GNSS smart antenna is used for obtaining SOTAB-II's position, velocity, and heading. The sensor can output data at a rate of 1, 2, 10, and 20 Hz. In this study, we are using an output data rate of 1 Hz to record the position of the buoy each second.
- ***Compass Sensor:*** For the azimuth, roll, and pitch angle of SOTAB-II, we are using a TDS01V, a 3D sensor that can measure onboard 3-axis accelerometer, 3-axis geomagnetic, and absolute atmosphere. The 3D sensor has a variable accuracy and range for obtaining roll, pitch, and azimuth angle. It can measure azimuth from 0° to 360° with clockwise positive, pitch angle from 0° to 45° and roll angle from -45° to 45°.

2.3.2 Oceanographic Sensors

- ***Wind Anemometer:*** The anemometer selected for SOTAB-II is ultrasonic wind anemometer manufactured by Gill Instruments: Environmental and Industrial Monitoring Solutions. For wind direction, the measurement is 0° to 360° if north to south, 90° east to west, 180° south to north, and 270° from west to east. The anemometer's wind speed and direction resolution are 0.01 m/s and 1°, respectively. The accuracies of the wind speed and direction were within ±2% and ±3°, respectively.
- ***Water Current Meter:*** For current meter, AEM-RS an electromagnetic current meter produced my Japan Alcc company is used. The current meter gives water velocity and compass readings with which the current velocity and direction can be calculated. The resolutions of the current speed and direction were 0.02 cm/s and 0.010, respectively. The measurement accuracies of the current speed and direction were within ±2% and ±2°, respectively. The results of sensor speed and direction calibration testing are published in Rathour et al. (2015a).

2.3.3 Communication

As explained above, SOTAB-II uses various sensors and actuators for its localization and actuation, each with a different communication protocol depending on the firmware implementation, RS-232, CAN, and USB protocols. Manual control of SOTAB-II is also possible via a wireless link, using a remote computer (Figure 2.3 (A)). For sending data to a land base station, SOTAB-II will use the iridium satellite communication network; although SOTAB-II does not presently have an iridium satellite antenna, it will be added in the near future.

2.4 Software Module

Figure 2.3 (B) shows an overview of SOTAB-II's software architecture. All software was written in Borland C++. This software manages a shared memory and thus provides communication between the individual sensor programs. For example, sensor drivers read the sensor data from the detector hardware and write it to the shared memory. Other programs requiring sensor data for processing can read data directly from the shared storage. The command signals generated by the GNC for sail and rudder control are likewise stored in the shared memory for further analysis (Figure 4.3 (B)).

2.4.1 Data Acquisition Module

Sensor data includes wind speed and direction, water current and direction, position, azimuth, and the relative position of SOTAB-II. These sensors each have their own acquisition frequencies and resolutions. To begin with, the collection and formatting of input data from the sensors is carried out by the onboard computer interfaced by the sensors by the data acquisition module. The data from each sensor is saved in the shared memory with a common clock giving a coherent sense of timing to all the measurements. Secondly, the environmental condition and relative position of SOTAB-II, with respect to the oil slick, is extracted from the sensors and fed to the GNC module.

2.4.2 Guidance, Navigation, and Control Module

The main objective of the GNC module is to reliably detect and localize the oil slick, and to supply the control actuators with real-time rudder angle and sail position instructions to achieve the target heading and target speed. Target heading and speed are computed based on the data from the oil sensor and environmental conditions (e.g., wind direction). The target heading is computed by way of a decision-making algorithm, which computes a new target heading each time the data coming from the data acquisition module is refreshed. The target heading is modified to compute the best feasible heading, considering physical constraints of SOTAB-II. The main sail position is computed based on the target speed and SOTAB-II's speed. The target heading and target speed derivation algorithm is described in detail in Section 5.1. The desired rudder angle and mainsail position, coming from the GNC module, is used as a reference for the PID controllers designed for controlling the rudder and mainsail. The PID control algorithm for mainsail and rudder is described in detail in Section 6.2.

3 Mathematical Modeling

3.1 Introduction

SOTAB-II has enough potential to prove itself as long term oil spill observer platform, because of using wind energy as propulsion energy. The main aim of the controller designed for SOTAB-II is to keep the drift velocity and the heading direction synchronized with the results or the decision taken based on the oil sensor data. However, the sole dependence of SOTAB-II on wind for tracking oil drift brings some limitation to the maneuvering characteristics of SOTAB-II and makes the system sluggish and difficult to control its motion due to the unreliable spatial and temporal distribution of wind. Mathematical models used for navigation and control of ships and underwater vehicles, can be found in the book by Fossen (2002). Xiao and Jouffroy (2014) followed a similar approach for dynamic modeling of sailboat. Sailing yatch or sailboat maneuvering model has been reported by various researchers. The work done by them generally deals with optimal tacking or rudder action for minimal speed loss during maneuvering e.g. IACC yachts (Ridder, 2004). Others have delineated the general maneuverability characteristics of sailing yachts under sail (Masuyama, 1993, 2011). The nonlinear behavior of sailboat while tacking and quick maneuvering motion accompanied by large rolling in short period of time was delineated by Masuyama et al. 1993.

3.2 Reference Systems

The mathematical model includes both hydrodynamic and aerodynamic forces affecting the system dynamics. Mathematical modeling of the dynamic system has proven itself as a most efficient and effective tool for simulating and analyzing the dynamics of

the system. In case of SOTAB-II the effective tracking of the oil slick is the main control target. For dynamic mathematical modeling of the SOTAB-II several assumptions were adopted, namely, the SOTAB-II is assumed to be rigid and have planar motion by neglecting heave motion, pitch motion and roll motion. Moreover, the linearized equations of motion are handled. The SOTAB-II is separated into parts containing main sail, jib sail, rudder, keel, brake board and hull, and the forces acting on the vehicle are summation of the influence of each component taken separately.

As described in Section 2.2, SOTAB-II uses various sensors for navigation. Altogether, SOTAB-II relies on five sensors for autonomous oil spill detection and tracking. Some sensor data is measured by an absolute value, such as GPS data using the earth coordinate; on the other hand, some data is defined by relative values, such as the wind speed measured by the anemometer, which only provides relative values in body coordinates. Consequently, it is necessary to coordinate between these disparate data forms by merging them into the same form. Coordinate systems are defined for the control system design by XY (i.e., earth fixed coordinate system) and xy (i.e., body fixed coordinate system) (Figure 3.1). Earth-fixed coordinate and body-fixed coordinate are defined in Figure 3.1. The origin of the body-fixed coordinate is assumed to coincide with the center of gravity of SOTAB-II. Vector addition of the measured data is carried out for coordinate transformation and a detailed implementation of the same can be found in coming subsection.

3.3 Model Equations

The velocity vector $V = [u, v, r]$ denotes the generalized surge, sway and yaw velocity vector in xy (body fixed) coordinate and $\eta = [X, Y, \theta]$ is position vector of

SOTAB-II with respect to XY (earth-fixed) coordinate. Hence the dynamic mathematical model expression describing the planar motion of SOTAB-II is given in Eqs. (3.1)- (3.3).

$$(\mathrm{m}+\mathrm{m}_x)\dot{u} = X_u u + \mathrm{X_E} \tag{3.1}$$

$$(\mathrm{m}+\mathrm{m}_y)\dot{v} = Y_v v + Y_{\dot{r}}\dot{r} + (Y_r - mU)r + Y_\delta \delta + Y_E \tag{3.2}$$

$$(I_{zz}+\mathrm{J}_{zz})\dot{r} = N_{\dot{v}}\dot{v} + N_v v + N_r r + N_\delta \delta + N_E \tag{3.3}$$

where $\mathrm{X_E}$, Y_E, N_E are the external forces and the moment acting on the SOTAB-II, respectively, m is the total mass of the system , m_x, m_y,are added mass in x, y directions, respectively, and I_{zz}, J_{zz} are moment of inertia and added moment of inertia, respectively. The remaining are the hydrodynamic derivatives whose values are given in Table 3.1.

3.4 Aerodynamic Modeling of Main Sail & Jib Sail

As shown in Eqs.(3.4)and (3.5) $C_L and\ C_D$ are coefficient of lift (L) and drag (D) for the sail, respectively, $\vec{W_r}$ is the relative velocity of the wind with respect to the vehicle, $(90-\gamma)$ is the angle of attack, S is instantaneous surface area of the sail and Xe is the external force acting on the vehicle exerted from the main sail.

$$\mathrm{L} = \frac{1}{2}\rho {W_r}^2 S C_L \tag{3.4}$$

$$\mathrm{D} = \frac{1}{2}\rho {W_r}^2 S C_D \tag{3.5}$$

$$Xe = L * \cos(90 - \gamma) + D * \sin(90 - \gamma) \qquad (3.6)$$

$$= \frac{1}{2}\rho S V^2 (C_L cos(90 - \gamma) + C_D \sin(90 - \gamma))$$

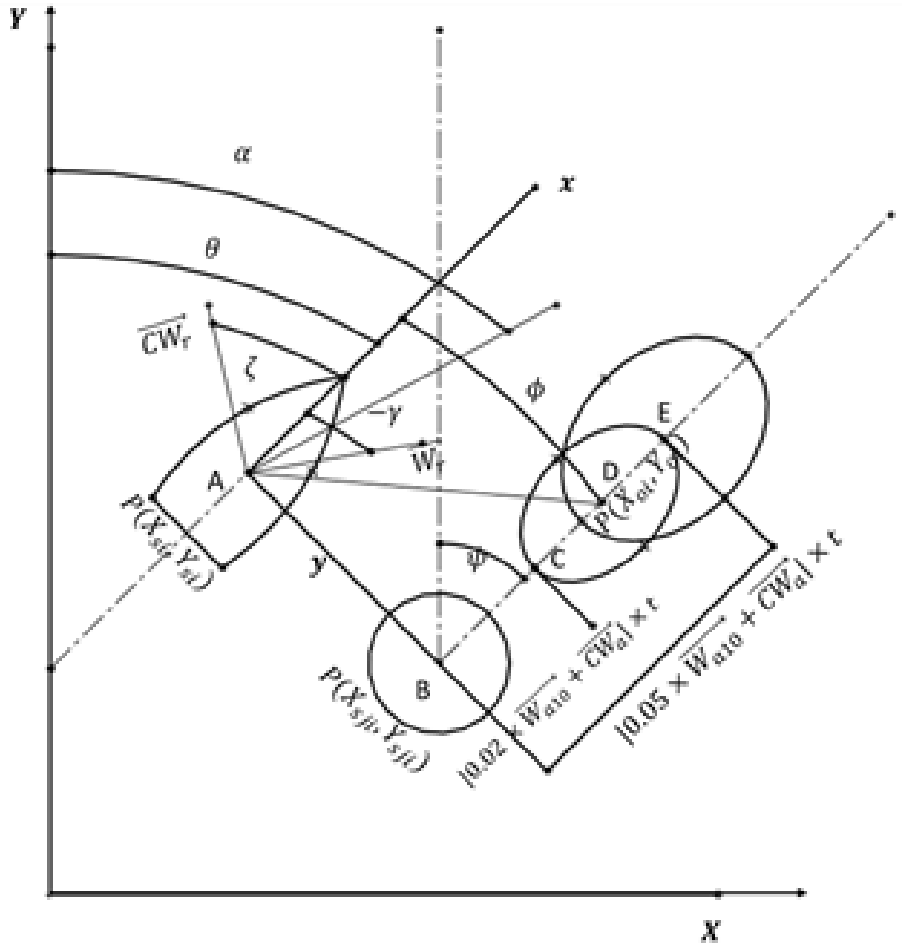

Figure 3.1 Reference system

In the same fashion the dynamics of the jib sail is described in Eqs. (3.7)- (3.8). below where γ denotes angle of attack, Ye the external force due to the jib sail in sway direction and Ne the yaw moment about the cg of the vehicle due to the sway force produced by the jib sail, and l the length to the center of jib sail from SOTAB-II center

of gravity.

$$Ye = 0.5\rho SV^2(C_L cos(\gamma) + C_D \sin^2(\gamma)) \quad (3.7)$$

$$\mathrm{Ne} = Ye * l \quad (3.8)$$

Using the above mentioned equations Simulink blocks were built separately for the jib sail and the main sail. Similarly the dynamic blocks for the rudder and the screw propeller were built. The rudder dynamics is already included in the maneuvering equation of Eqs. (3.1)- (3.3).

3.5 Comparison of Simulation and Experiment

System identification and parameter identification are a powerful tools that allows researchers to use real time data to estimate model parameters which can be used for control system design. System identification and model parameter identification techniques have been used widely by aerospace industry and various other robotic and control field. This technique has been used to classify a dynamic system handling qualities, controller development for autonomous flight systems ((Morelli, et al., 2005, Jategaonkar, 2006).

Autonomous sailboat is a complex system to model with respect to control prospective, as it involve highly nonlinear hydrodynamic and aerodynamic parameters. As SOTAB-II is wind powered autonomous surface vehicle, the nonlinear behavior of wind makes its highly vulnerable to environmental conditions. The augmentation of SOTAB-II with appendages such as brake board below the water line, rotating oil sensor and sail makes it even more complex. Building an autonomous controller for such a complex system is a challenge.

For the development of non-linear steering and maneuvering model of ship naval architectures has been using system identification technique since 1960 (K. Nomoto, 1957; K. Nomoto, et. al.,1960). Basically there are two common maneuvers that are used for estimation and validation of the non-linear hydrodynamic derivatives: the circle test and the zig-zag maneuver. In case autonomous sailboat the circle test cannot be performed, as it is difficult for a sailboat to sail in a perfect circle and also non-linearity of wind in both time and space makes impossible to maintain constant thrust during such maneuver. Similar difficulties is encountered in case of zig-zag test too, as it is difficult to maintain constant thrust. For model parameter identification and controller design, the time history of the wind sensor, rudder position and the main sail length was used as an input data set to the system. For the comparison of estimated and measured experimental data for hydrodynamic parameter identification the software MATLAB was used. Hydrodynamic and aerodynamic coefficients of SOTAB-II were estimated from the experimental data using parameter identification (nonlinear least square method). The physics based dynamic model as described in Eqs. (3.1-3.3) was implemented in Simulink Matlab (Figure. 3.2). When the Simulink model is given the current environmental state of wind, sail and rudder as input, the derivative of each SOTAB-II state is returned which is integrated further for speed over ground (V) and azimuth (θ) estimation. Further, the estimated V and θ was compared with the measured speed and azimuth of SOTAB-II, the error between the measurements and estimated data derived from the simulation was minimized using non-linear least square method to update the unknown hydrodynamic parameter. The process was repeated until the saturation in hydrodynamic parameter was achieved.

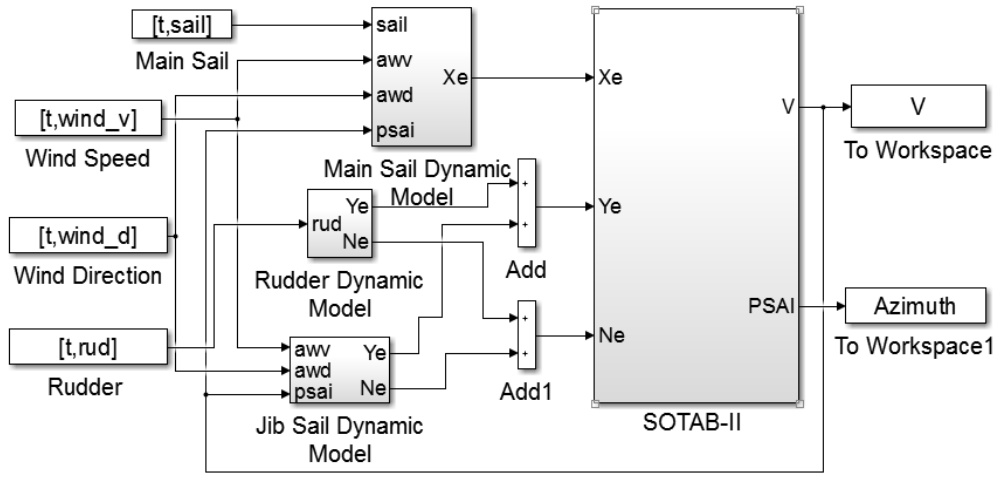

Figure 3.2 SOTAB-II Mathematical model

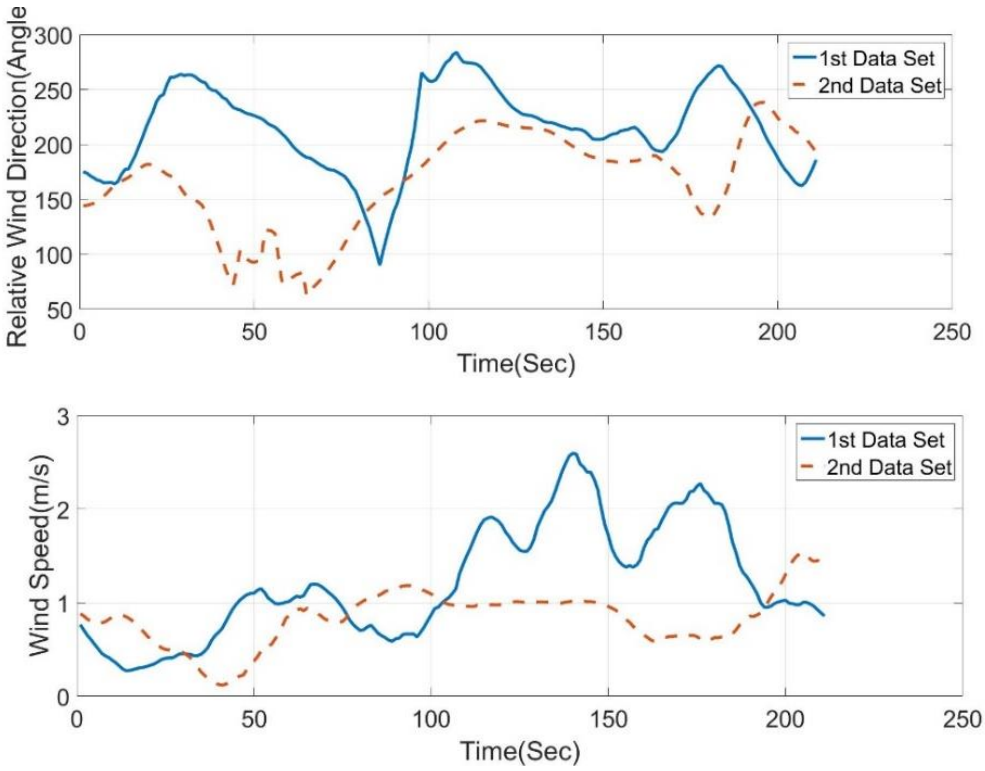

Figure 3.3 Input wind data set for parameter identification

For parameter identification, control drift experiments were carried out in pond, with fixed sail and varying the rudder angle. For this parameter identification two set of input data and output data set was used. Input data and output data used for parameter

identification are shown in Figure.3.2. $Y_{\dot{r}}$, $N_{\dot{v}}$ has been neglected as SOTAB-II is slow moving. From the first data set hydrodynamic parameters were estimated, second data set was used to validate the estimated hydrodynamic parameters. Figures 3.3 and 3.4 show the measured and simulated data for first data set and second data set respectively. The estimated hydrodynamic coefficients are shown in table 3.1. The simulated output data (i.e. SOTAB-II speed over ground and azimuth) using estimated hydrodynamic parameter show good correlation with the experimental data.

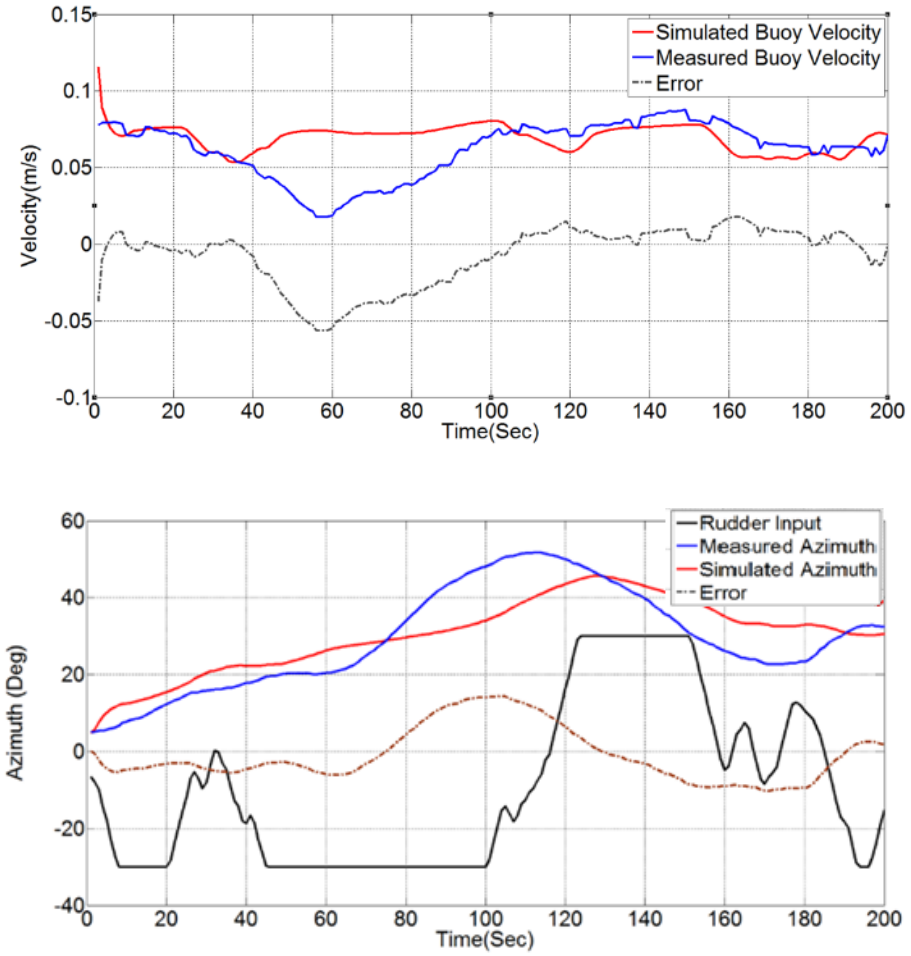

Figure 3.4 Motion behavior of SOTAB-II (Top) estimated velocity and measured velocity, (Bottom) simulated and measured azimuth and measured time history of rudder angle for 1st data set.

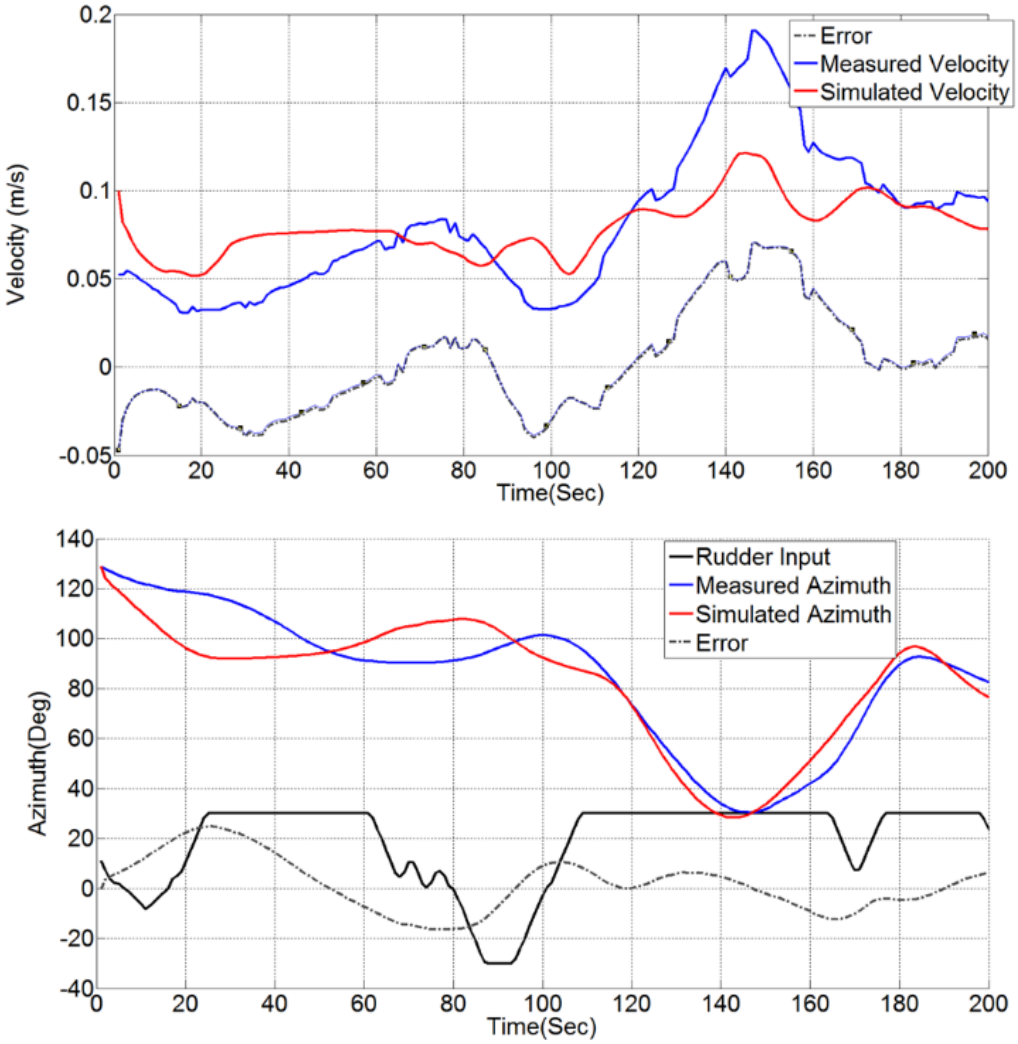

Figure 3.5 Motion behavior of SOTAB-II (Top) estimated velocity and measured velocity, (Bottom) simulated and measured azimuth and measured time history of rudder angle for 2nd data set

Table 3-1 Values of hydrodynamic derivatives of SOTAB-II

Hydrodynamic Derivatives	Numeric Values
Xu (N · s/m)	-26.8648
Mx(Kg)	6.815041
My(Kg)	54.63201
Yv (N · s/m)	-324.03
Nv(N · s)	15.40323
Nv`(N · s^2)	0.607915
Yr`(N · s^2)	-1.73668
Yr(N · s)	27.61932
Jzz(Kg-m^2)	14.63696
Nr(N · s · m)	-126.347
Yδ(N)	-0.33497
Nδ(N · m)	0.169763
Izz(Kg-m^2)	26.52419
m(kg)	90

4 Sensor Calibration

4.1 Water Current Sensor Calibration

For in situ measurement and observation of ocean currents, SOTAB-II is equipped with an AEM-RS a two dimensional electromagnetic water current velocity meter. The AEM-RS sensor was calibrated in a model basin tank at Osaka University. As shown in Figure 4.1 (A & B), SOTAB-II was fixed on the towing tank carriage before being moved at speeds of 0.1m/s to 0.5m/s for calibration, during which current sensor information was logged for offline analysis. Figure 4.2 shows the lateral and longitudinal measured current strength against the carriage speed with brake on and brake off. The lateral measured current in both brake on and off condition was found to be similar whereas an offset was observed in longitudinal measured current with brake off condition.

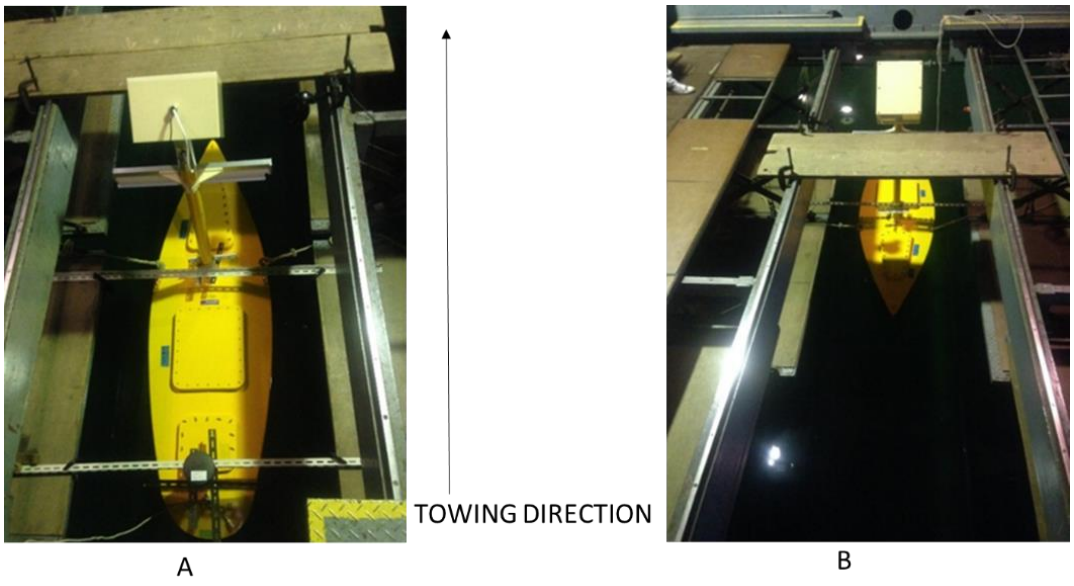

Figure 4.1 Experimental setup for current sensor calibration

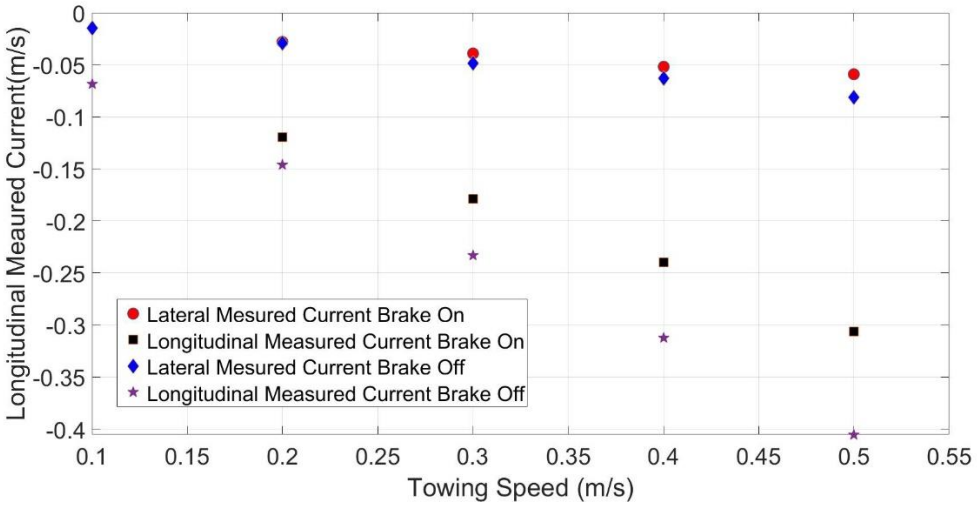

Figure 4.2 Water Current Sensor Calibration

Brake Board On

$$CW_{ax} = CW_{rx} - (-0.105 \times V - 0.0077) \quad (4.1)$$

$$CW_{aY} = CW_{rY} - (-0.621 \times V - 0.0063) \quad (4.2)$$

Brake Board Off

$$CW_{ax} = CW_{rx} - (-0.167 \times V - 0.0029) \quad (4.3)$$

$$CW_{aY} = CW_{rY} - (-0.845 \times V - 0.0190) \quad (4.4)$$

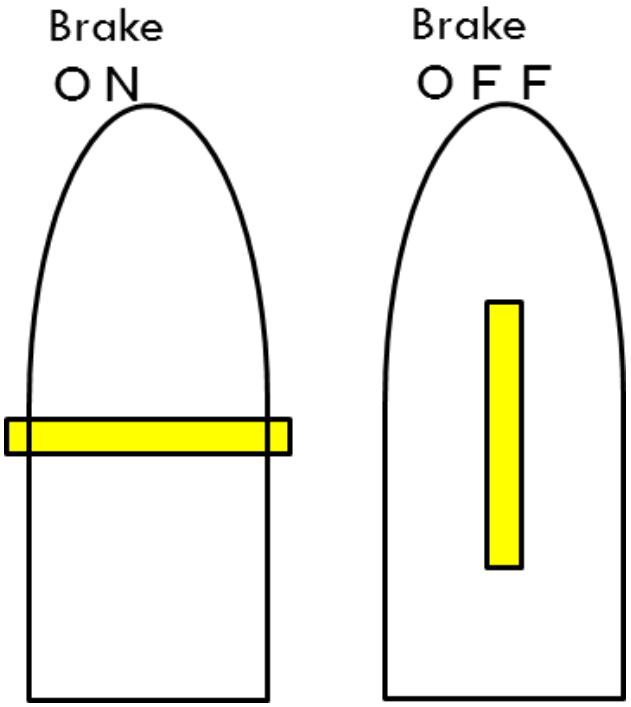

Figure 4.3 Orientation of brake board with respect to SOTAB-II hull in case of ON and OFF position respectively

Hence, in real time water current measurement the error in water current measurement due to SOTAB-II motion need to be adjusted as per Figure 4.2 (Eq. (4.1-4.2) in case of brake board on, and Eq. (4.3-4.4) for brake board off). Figure 4.4(top & bottom) shows measured ocean water current and estimated water current during a sea experiment conducted at Eigashima beach, Kobe on 26th January 2016. During the ocean current observation it was found that the heave, yaw and roll motion induced some error in the water current observation, it was decided to use a kalman filter for smoothing the measured water current.

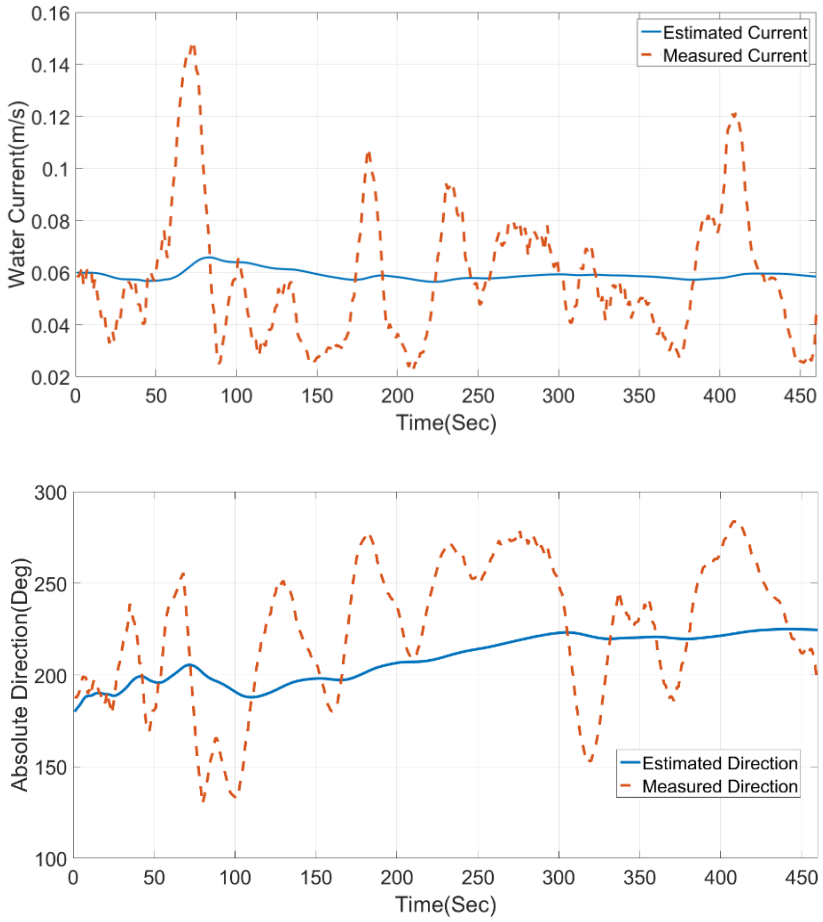

Figure 4.4 (Top) Water current estimation (Top) Water Current speed estimation, (bottom) Water Current direction estimation

4.2 Oil Sensor Calibration

SOTAB-II uses an optical-based Slick Sleuth SS300 (InterOcean System) as an oil detection sensor. The optical-based oil sensor detects the fluorescence of oil. The oil sensor has an onboard receiver, transmitter, and detecting circuit. The sensor transmits a cone-shaped beam of ultraviolet rays at an angle of 14deg at the target to be monitored (Figure 4.5 (c)). After absorbing the ultraviolet rays, the target emits light in the visible spectrum, which is then captured by the receiver. If the captured fluorescence matches

the oil fluorescence, the sensor generates a pulse verifying the presence of petroleum. Different oils will have different fluorescence values; therefore, the sensor sets the threshold of the detecting circuit according to user requirements.

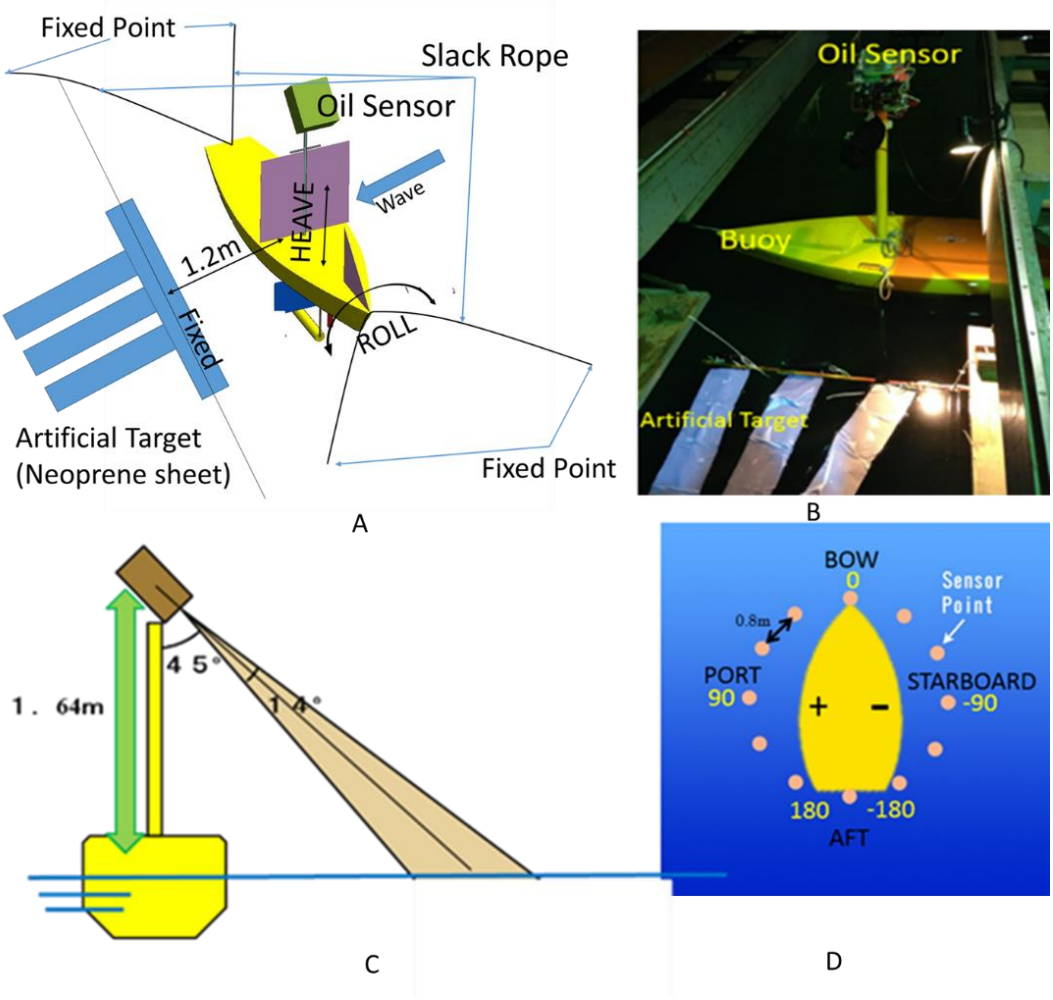

Figure 4.5 Calibration of oil sensor (A) Schematic of experimental setup, (B) Experimental setup, (C) Oil sensor zone for detection of oil slick, (D) Oil sensor reference axis with respect to buoy.

Oil sensor performance was tested in the Osaka University model basin. The oil sensor was mounted on the SOTAB-II as shown in Figure 4.5 (A & B). Waves were generated and the SOTAB-II was placed facing the beam waves so that the performance

of the oil sensor could be checked in the relative motion between the artificial target and SOTAB-II. The experimental setup is shown in Figure 4.5 (A). The degree of freedom of the buoy was constrained to allow for roll and heaving motions using slack cables. For the artificial target, white fabric pasted on neoprene sheets, which can float freely on the water surface, was used. This model of target was chosen because the oil sensor can give a false signal when focused on white fabric (Mahr & Chase, 2009). Three 1m long target sheets were constructed, with one end of the sheet fixed to a rod and the other end kept loose so that the sheets could follow the wave profile. The sensor can reliably detect and signal the presence of oil in a 2–5m range. If the distance between the oil sensor and the oil slick is greater than 5m due of the relative relationship between the attitude of the SOTAB-II and the wave profile, the sensor reading cannot be accepted for target detection. The experimental roll motion results in Figure 4.6 (A) are indicated for a wave with a wavelength of 10m and a height of 0.05m. The artificial target was located at the periphery of the circle with a radius of 1.2m from the SOTAB-II center. The threshold value was first measured from the water surface without the white sheets. The results of the experiment are shown in Figure 4.6 (B), where sensor reading above 25000 corresponding to oil detection and a reads below 25000 suggests the absence of oil on the targeted surface. As shown in Figure 4.6(A, B), the sensor was not capable of detecting the artificial target when the roll angle of the buoy exceeded 10–12 degrees.

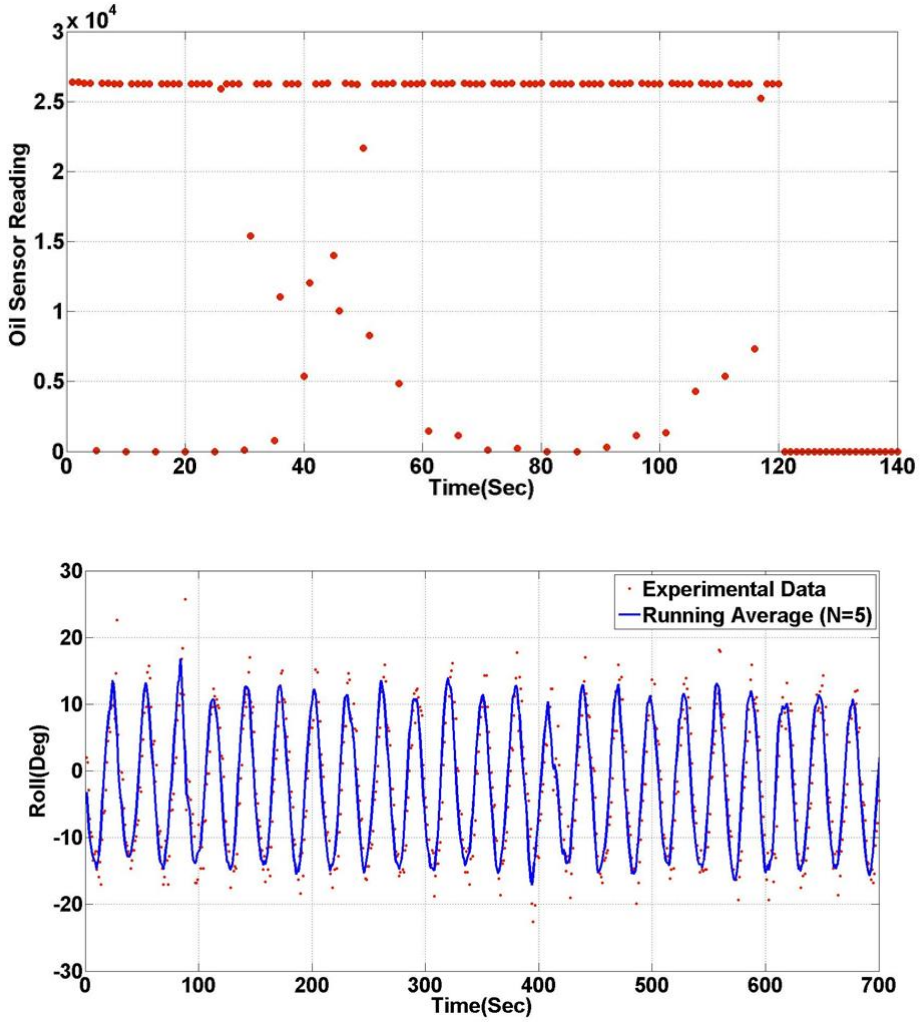

Figure 4.6 Oil sensor reading in rolling motion of SOTAB-II (A) Buoy azimuth sensor data for roll motion (original data and running average data for smoothing), (B) Oil sensor reading.

5 Decision Making Algorithm

5.1 Introduction

As described previously, SOTAB-II uses various sensors for navigation. This section describes the decision-making process for deriving the control input from the sensor information. Altogether, SOTAB-II relies on five sensors for autonomous oil spill detection and tracking. The heading and speed of SOTAB-II is decided after determining the robot's present position relative to the oil slick as determined based the on oil sensor data. The main objective of the decision algorithm is to keep track of the oil slick, in case SOTAB-II loses the track of oil slick.

The effect of wind drift factor on the spread and drift of oil spill varies from 0.02-0.06. This makes the estimation of oil slick position with time challenging. Because the percentage of the wind velocity is not an exact value is yet to be confirmed or validated in our lab, as a matter of temporary expedience, we set a hypothetical wind velocity of 3.0% i.e. $(0.03 * \overrightarrow{W}_{a10})$ at a height of 10m from the sea surface as the wind effect on the drifting velocity of an oil spill. Nevertheless, as shown in Fig 3.1 if oil slick at point B drift with 2% wind drift factor, it may end up at point C, and if the wind drift factor is 5% it may end up at point E. Hence, if wind speed is 40m/s the maximum uncertainty of oil spill drift will be within 7m (considering 1m/s water current strength) in 3 sec. This uncertainty in drift distance can be easily covered up by SOTAB-II length, if SOTAB-II is made to track the oil slick drifting with wind drift factor of 0.03.

5.2 Decision Making Algorithm

SOTAB-II uses an optical-based oil detection sensor that detects the fluorescence of oil. The sensor transmits a cone-shaped beam of ultraviolet light at an angle of 14° to the target to be monitored. After absorbing the ultraviolet rays, the target reflects light in the visible spectrum, which is then captured by the receiver. If the captured fluorescence matches the oil fluorescence, the sensor generates a pulse verifying the presence of petroleum. Different oils will have different fluorescence values; therefore, the sensor sets the threshold of the detecting circuit according to user requirements. Based on the data received from the oil sensor, the decision-making algorithm can determine whether the robot is moving away from or drifting with the oil slick. Because oil sensor can be focused on a small area, it was decided to rotate the oil sensor by 360° to cover the area around SOTAB-II. This circular target area is divided into 12 sectors of 30°as shown in Figure 5.1 (A).

$$P_i = \{s_0, s_1, s_2, \dots s_{12}\}, s_j = 1 \; or \; 0 \; (j = 0,1,2,3,\dots 13) \tag{5.1}$$

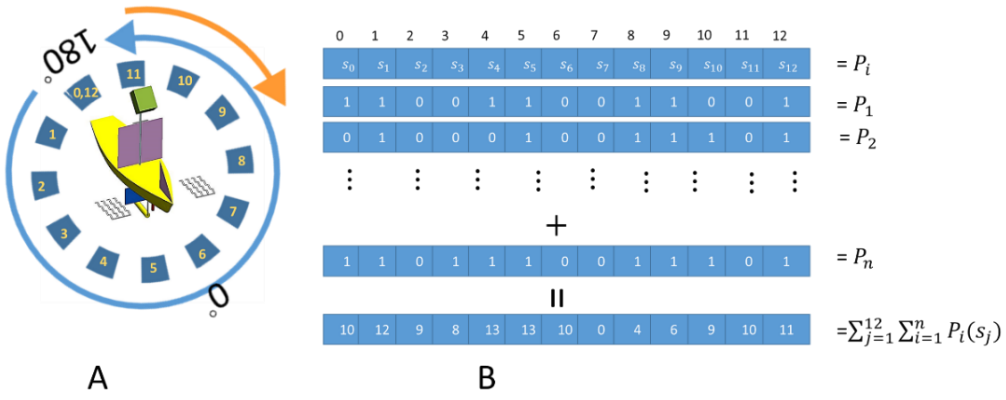

Figure 5.1 Data management of oil sensor (A) Target scan area and target points, (B) Time history sensor dataset and current sensor dataset

The oil sensor is rotated continuously in a footprint of 30° to skim the area around the SOTAB-II. It takes 2 s for the mast to rotate the oil sensor by 30° and 1 s to take a reading of the target area (Figure 5.1 (A)). For each scan, the circular position of the oil sensor and its reading is stored in the shared memory. The positional value of the oil sensor is defined in respect to the body axis frame with the absolute angular position shown in Figure 5.1 (A).

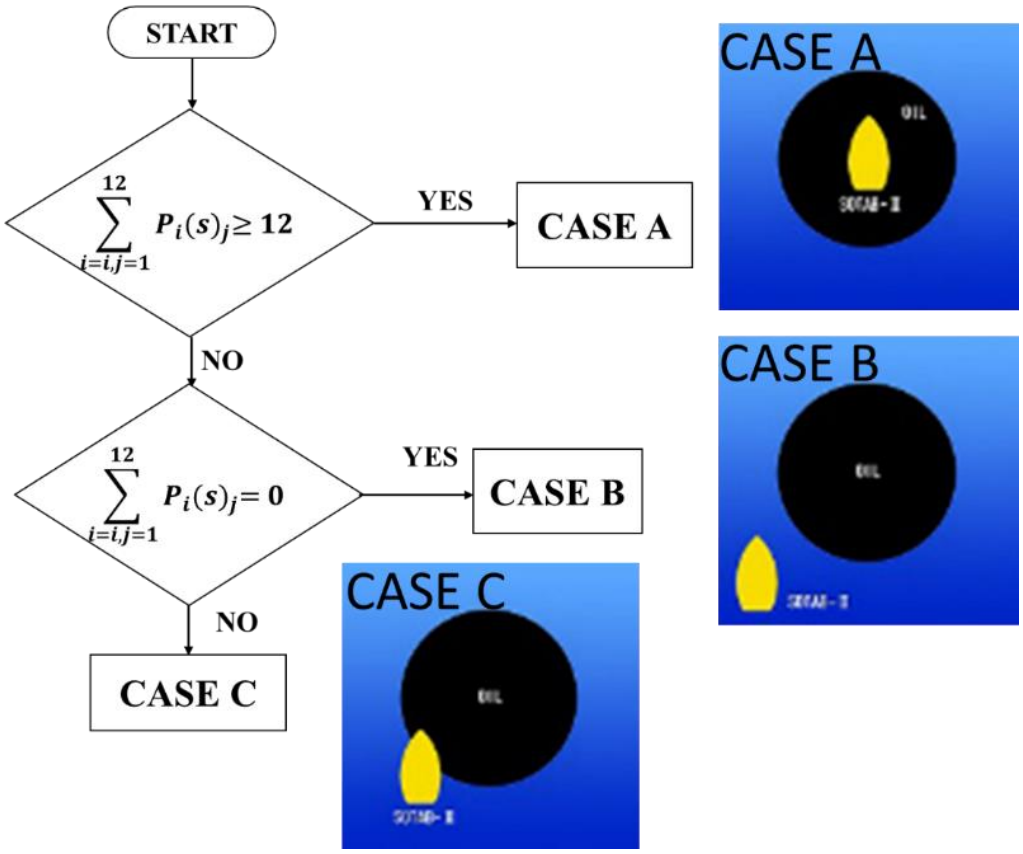

Figure 5.2 Decision algorithm flowchart

The target heading and target speed of SOTAB-II is decided after determining the robot's present position relative to the oil slick as determined based the on the oil sensor data. Figure 5.2 shows an overview of the decision-making algorithm. Thirteen readings need to be taken around the SOTAB-II to determine whether the robot is within the spill,

out of the spill, or at the border of the spill. To calculate the target heading (TD) and target speed (TV), the maximum number of detected sensor points is computed (Figure 5.1 (A)). The 13 readings for one complete rotation of the oil sensor are expressed in Eq. (5.1). P_i in (5.5) represents the oil sensor data set for one rotation of the oil sensor, where 1 denotes successful oil detection and 0 denotes a failure to detect oil. At the start of the experiment, the decision-making algorithm initially waits for the first sensor data set $P_{i=1}$, after which P_i is updated every 3 s as it takes 3 s for the sensor to move to a new position and compute the target area reading (s_j, Figure 5.1(A)). Based on the maximum number of detected sensor points in sensor data set (i.e., $\sum P_i(s_j)$ in each P_i (Figure 5.1 (B)), and the time history of the cumulative sum of sensor data for each of the target points expressed in Eq. (5.1) (i.e.,$\sum_{j=1}^{12}\sum_{i=1}^{n} P_i(s_j)$ (Figure 4.5 (B)), the following rules were derived:

5.2.1 Case A (Target Heading and Target speed derivation if SOTAB-II is surrounded by oil):

If all 13 readings expressed in Eq. (5.1), are true and oil is detected by the oil sensor (i.e., $\sum s_j \geq 12$ Figure.5.2), then it can be concluded that SOTAB-II lies within the oil spill. As long as SOTAB-II is within the oil spill, TD and TV will be calculated as follows:

$$TD = \psi \text{, Where } \psi = \angle(\overrightarrow{w_{a10}}, \overrightarrow{cw_a}) \tag{5.2}$$

$$TV = |0.03\overrightarrow{w_{a10}} + \overrightarrow{cw_a}| \tag{5.3}$$

$$p(x_{oi}, y_{oi}) = p(x_{si}, y_{si}) \tag{5.4}$$

5.2.2 Case B (Target Heading and Target speed derivation if SOTAB-II is out of oil slick):

If all the 13 readings expressed in Eq. (5.1) are not true and oil is not detected by the oil sensor (i.e., $\sum s_j = 0$), then it can be concluded that SOTAB-II lies out of the oil spill (Figure.5.2). In such a situation, from the time history of the oil sensor dataset, $p(x_{oi}, y_{oi})$ can be derived, the best known position of SOTAB-II where oil was found. Furthermore, if SOTAB-II is made to converge upon the line defined by the waypoint $p(x_{oi}, y_{oi})$ where oil was detected and the slope of the line is given by the resultant direction of the water current and wind (ψ), SOTAB-II can be guided back to the oil slick. Equation 5.5 gives the formula to find the oil slick position, in case if SOTAB-II continues to be in CASE B condition. Hence if $\sum p_{i-1}(s_j) = 0$ and $\sum p_i(s_j) = 0$, then the $(i-1)$ estimated oil slick position (5.6-5.9) gives the oil slick absolute position.

$$p(x_{oi}, y_{oi}) = \begin{cases} p(x_{sij}, y_{sij}) & \text{if } \sum p_{i-1} \neq 0 \text{ and } \sum p_i = 0 \\ p(x_{oe(i-1)}, y_{oe(i-1)}) & \text{if } \sum p_{i-1} = 0 \text{ and } \sum p_i = 0 \end{cases} \quad (5.5)$$

$$p(x_{oei}) = p(x_{oi}) + TV \times t \times \cos(\psi) \quad (5.6)$$

$$p(y_{oei}) = p(y_{oi}) + TV \times t \times \sin(\psi) \quad (5.7)$$

$$\emptyset = atan2(p(y_{oei}), p(x_{oei})) \quad (5.8)$$

$$TD = \theta - \emptyset \quad (5.9)$$

In case $\sum p_{i-1}(s_j) \neq 0$ and $\sum p_i(s_j) = 0$ (change in case from A&C to B), then the SOTAB-II absolute position where the $\sum_{j=1}^{12} \sum_{i=1}^{n} P_i(s_j)$ was maximum before losing the oil slick gives the oil slick position (Eq. 5.5) first case, subscript j in $p(x_{sij}, y_{sij})$ is to point out the location where SOTAB-II lost the track of oil scanning the target point with largest cumulative sum). This is same as a look ahead-based line-of-sight (LOS)

algorithm (Lekkas, 2012). The waypoint $(p(x_{oei)}, y_{oei}))$ (5.6-5.9) is kept on projecting by a distance defined by $(t \times TV)$, t is algorithm update time, unless SOTAB-II finds the oil slick. In this case the TD is stated in (5.9). $\emptyset$ in (5.8) represents the bearing of the estimated oil spill location from the SOTAB-II absolute position.

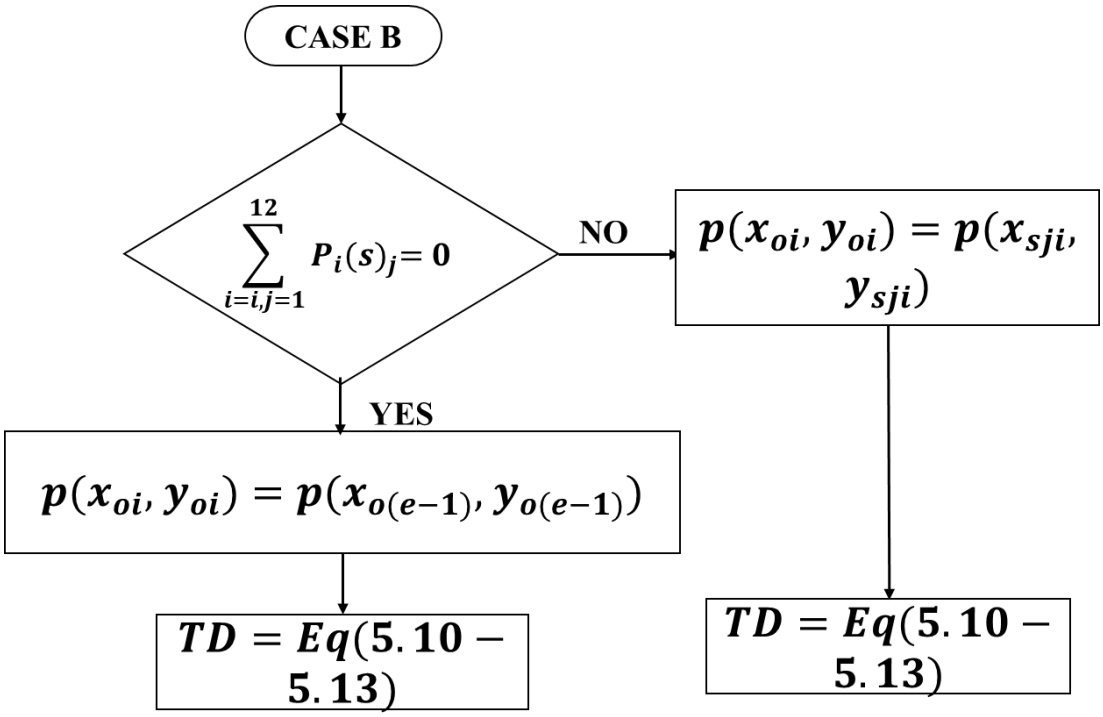

Figure 5.3 Case B flow chart

5.2.3 Case C (Target Heading and Target speed derivation if SOTAB-II is tracking the edge of the oil slick):

If the number of true sensor readings is less than 12 (i.e., $\sum_{j=1}^{12} P_i(s_j)$ <12, Figure.5.2), it implies that SOTAB-II lies on the edge of the spill. Figure 5.6, shows the clustering algorithm used to deduceTD. The bar in the Figure 5.6 shows $\sum_{j=1}^{12}\sum_{i=1}^{n} P_i(s_j)$ and circle near the edge of the bar shows the detected points. Based on the relative position of SOTAB-II with respect to the oil slick, various conditions can be defined.

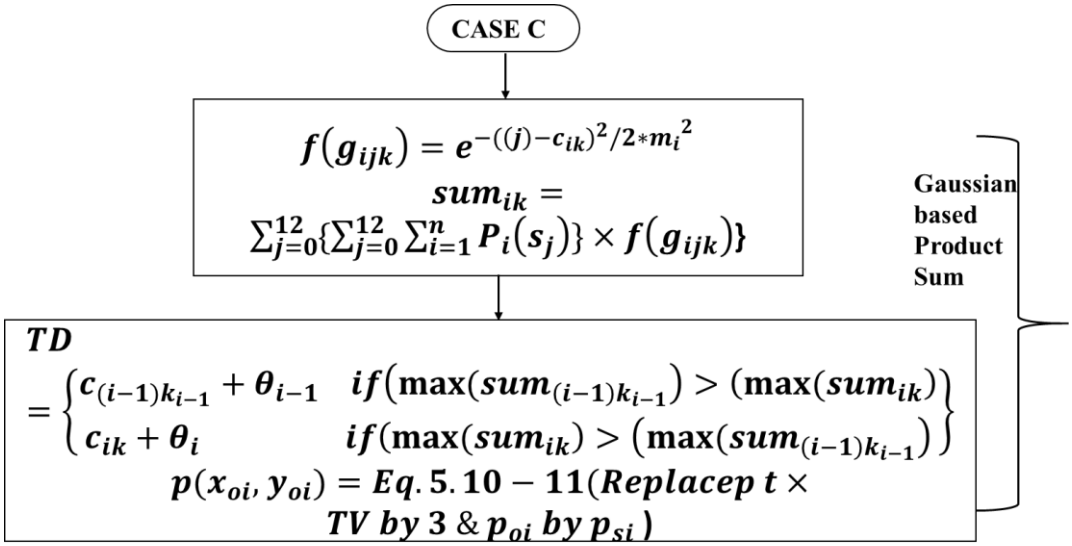

Figure 5.4 Case C flow chart

- ***Clustering Algorithm***: To deal with the worst case situation (i.e., where SOTAB-II is found to be surrounded with multiple patches of different sized of slicks), the sensor dataset (P_i) is scanned to determine the total number of large oil slick patches surrounding SOTAB-II (i.e.k). Therefore, the total number of clusters surrounding SOTAB-II is given by k and the center of each cluster can be derived using (Eq.5.11).

- ***Gaussian based oil slick cluster filtering:*** The center of each slick patch gives the Gaussian function mean (c_{ik}, (5.11)), and the length of the detected target point in each cluster of oil slick patch gives the standard deviation of the Gaussian function (m_i). In (5.11), j_{ik} is the starting indices of oil slick cluster subarray having k_i number of detected points. The Gaussian function dataset formed using (5.11), is multiplied element-wise, with the cumulative sum of target points

(or time history of target points (i.e.$\sum_{j=1}^{12}\sum_{i=1}^{n}P_i(s_j)$); (5.12). The total product sum of the element-wise multiplication of $\sum_{j=1}^{12}\sum_{i=1}^{n}P_i(s_j)$ and Gaussian functions (5.13) was compared to find the largest product sum (sum_{ik}). Target heading (TD) is given by the center of the oil slick patch having largest product sum using (5.13).

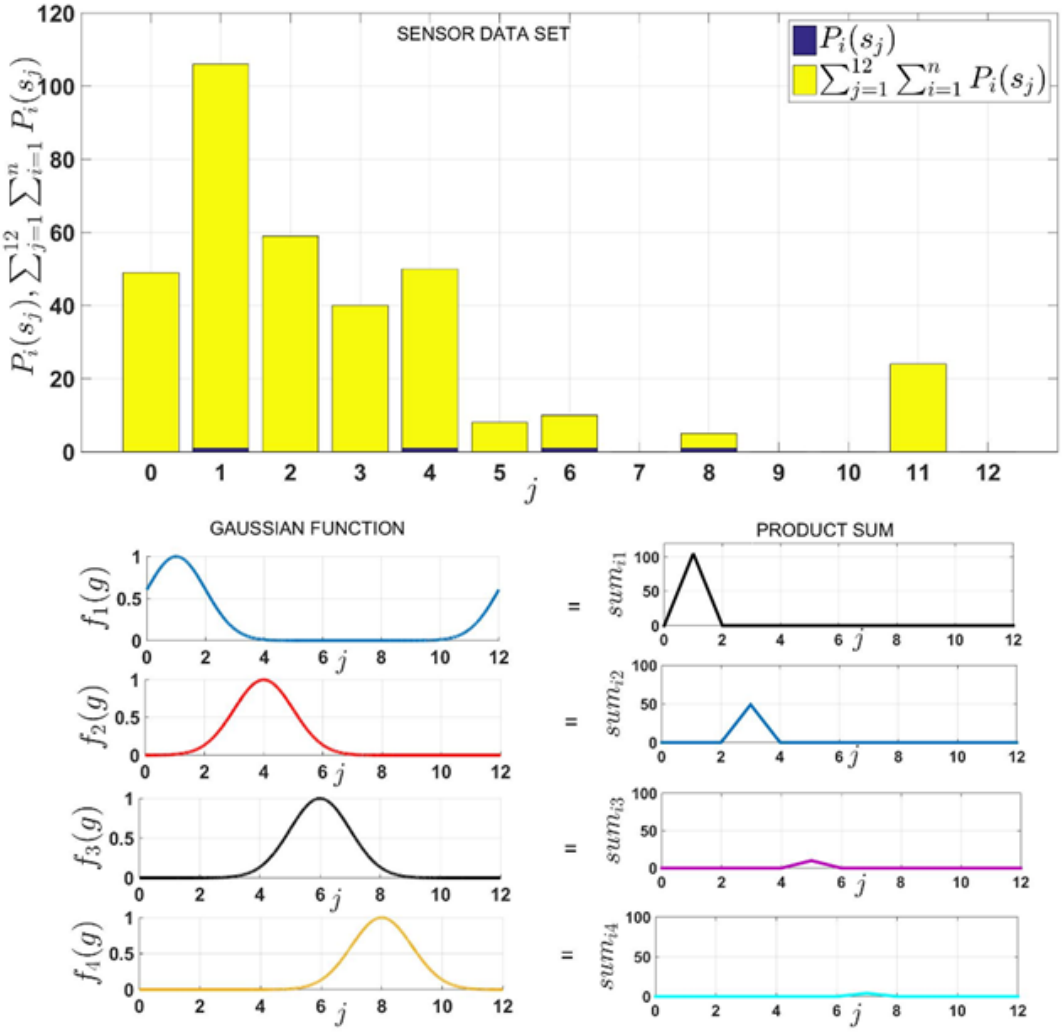

Figure 5.5 Gaussian-based product sum to derive target heading

$$f(g_{ik}) = e^{-((u)-c_{ik})^2/2*m_i{}^2} \qquad \text{Where}$$

$$u = \begin{cases} j - c_{ik} & if \quad (abs(j - c_{ik}) \leq 6 \\ (6 + c_{ik}) - abs(6 - j) & if \quad (abs(j - c_{ik}) > 6 \end{cases} \qquad j = 0,1 \ldots\ldots 12$$

(5.10)

$$c_{ik} = \frac{2*j_{ik}+m_i-1}{2} \qquad k = 1,2,\ldots.k_i \tag{5.11}$$

$$sum_{ik} = \sum_{j=0}^{12}\{\sum_{j=0}^{12}\sum_{i=1}^{n} P_i(s_j)\} \times f(g_{ik}) \tag{5.12}$$

$$TD = \begin{Bmatrix} c_{(i-1)k_{i-1}} + \theta_{i-1}, if\left(\max(sum_{(i-1)k_{i-1}}\right) > (\max(sum_{ik}) \\ c_{ik} + \theta_i \qquad if(\max(sum_{ik}) > \left(\max(sum_{(i-1)k_{i-1}}\right) \end{Bmatrix} \tag{5.13}$$

As the mathematical average of the angular position of target points within the group having largest sum_{ik} will be target heading. Target heading will be given by (5.13). In case of Case C oil slick absolute position will be given by (Eqs. 5.6-5.7), by substituting $t \times TV$ by 3, p_{oi} by p_{si} and ψ by $(TD + \theta)$ in (5.5-5.6).

6 Guidance & Navigation

This chapter introduces the oil spill tracking and how the target direction derived using decision control algorithm can be used for tracking oil spill as well as enclosing the oil spill using multiple SOTAB-II with limited communication.

6.1 Guidance and Navigation

Over the years, several methods have been proposed for the path plaining of wind-propelled vehicles, the majority of which have been based on fuzzy control theory, neural networks, or other artificial intelligence techniques (Abril et al. 1997; Stelzer et al. 2007; Stelzer and Proll, 2008). Local path planning using the potential method (Petres et al. 2011; Plumet et al. 2014), was also used to navigate the sailboat. However, in all the aforementioned work, none of these studies used a ship's dynamic equation. Other studies, such as Cruz and Alves (2010), used a model with three degrees of freedom for controlling the heading of the sailboat. Nevertheless, the highly nonlinear dynamic model of sailboats, due to complex hull aero- and hydrodynamic models, combined with various appendages (e.g., sail, keel, and rudder), is not always suitable for optimal control of sailing vessels. The use of wind and water current for propulsion of the ASV poses a significant limitation to for sailing vessels, as the vessels lose their propulsive force from the environment as they enter "no-go-zones", or zones or both upwind and downwind (Plumet et al. 2014; Stelzer et al. 2008). The sailing vessel can get stuck in a no-go-zone if it enters too slowly. Following the sailboat behavior described in the aforementioned work, the circular oil sensor target zone was divided into three zones (Figure 6.1 (B)). The objective is to steer the SOTAB-II toward the center of the slick whenever it tries to

go along the edge of the oil slick, avoiding upwind. With this objective in mind, the modified target heading (TD') and modified target speed (TV') was derived based on the region in which target heading lies and the wind heading in body coordinate. For navigation of SOTAB-II, wind heading in body coordinate was converted to $-180 \leq \gamma \leq 180$, with this range conversion of wind heading, oil senor target points, and wind heading will read negative starboard side and positive port side. TD' and TV' will be determined using the following rules (6.1–6.5):

$$TD' = TD \text{ if } (|TD| \leq 75) \vee ((75 < |TD| < 150)\ and\ ((\gamma \times TD) > 0)) \quad (6.1)$$

$$TD' = TD + 180 \text{ if } |TD| \geq 150 \quad (6.2)$$

$$TD' = 180 - \gamma \text{ if } 75 < |TD| < 150 \text{ and } ((\gamma \times TD) < 0) \quad (6.3)$$

$$TV' = TV + 0.1\%|(2 - 5\%)\overrightarrow{w_a} + \overrightarrow{cw_a}| \text{ if } |TD| \leq 75 \quad (6.4)$$

$$TV' = TV - 0.1\%|(2 - 5\%)\overrightarrow{w_a} + \overrightarrow{cw_a}| \text{ if } |TD| \geq 105 \quad (6.5)$$

6.2 Control

SOTAB-II aims to track the oil spill by continuously keeping itself surrounded by the oil that it is tracking. In our control system layout, the rudder and mainsail are modelled as separate Single Input and Single Output (SISO) systems, and proved to be reasonable during testing (Figure 6.2).

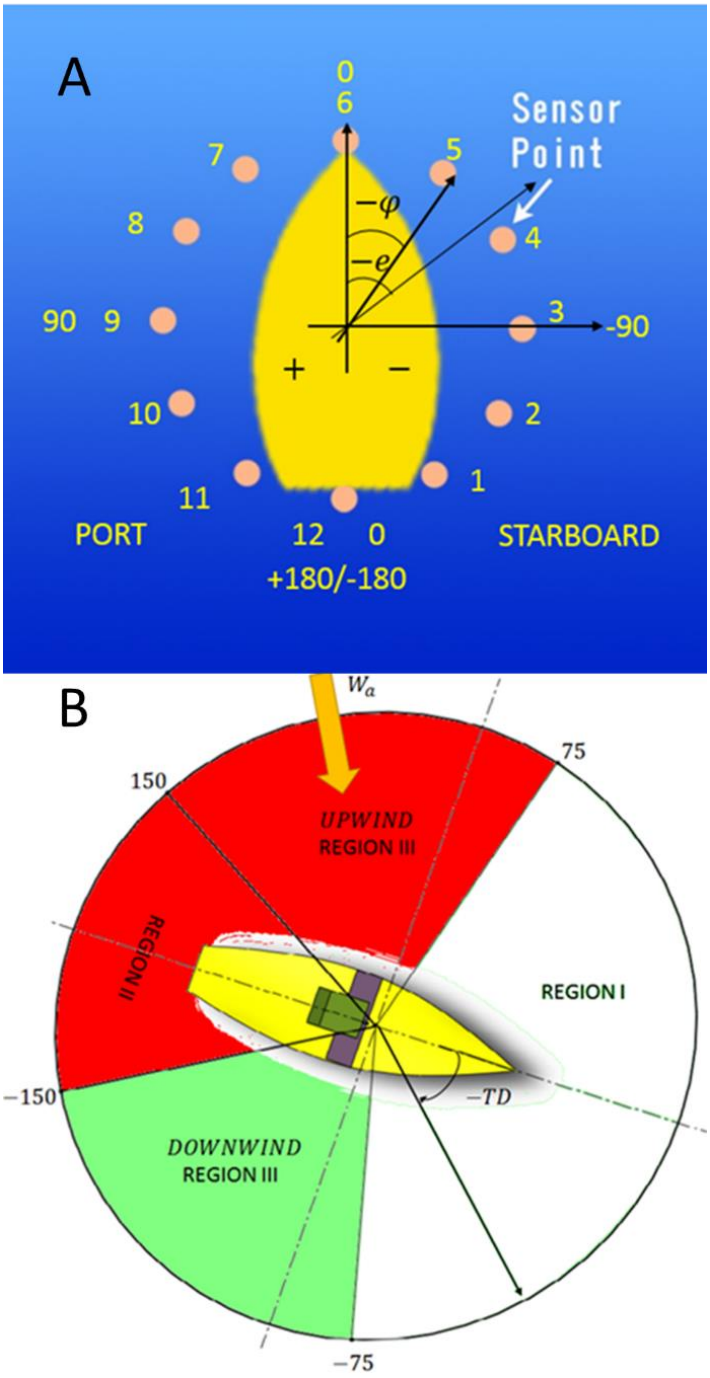

Figure 6.1 Circular oil sensor target zone (A) Oil sensor target points, (B) Division of circular zone around SOTAB-II for navigation

6.2.1 Sail Control

As explained above, the drift velocity of SOTAB-II depends solely upon the mainsail. The sail length is controlled via a PID controller (Figure 6.2). The control value for the mainsail is its length. The reference value is derived from the perception algorithm, which is further modified by the navigation module. TV', derived from the oil sensor dataset, acts as a reference point for the PID controller. Moreover, SOTAB-II's drifting speed (i.e., V) provides the feedback for the PID loop. If $V > TV'$, then the sail area is reduced, and if $V < TV'$, the sail area is increased.

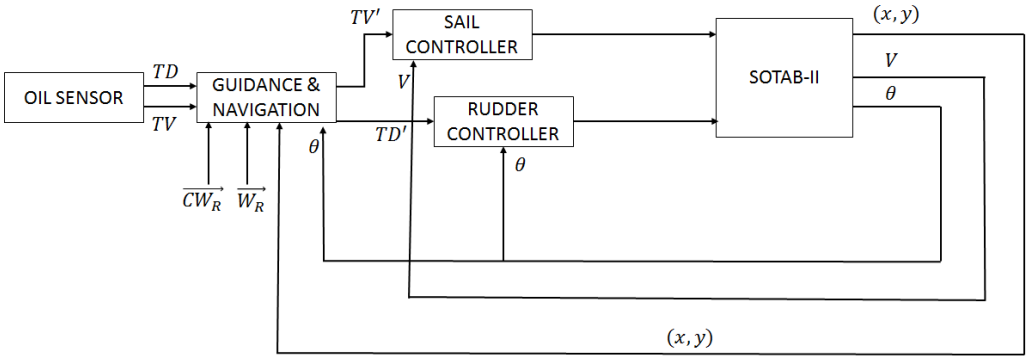

Figure 6.2 Control flow diagram

6.2.2 Rudder Control

The maximum rudder angle is limited to $\pm 30°$ Rudder motor control signals are generated by the PID controller where a heading error (e) is in the range of $\pm 20°$; if out of this, a rudder range control signal of $\pm 30°$ is generated based on the e sign (Figure 6.1 (A)). Therefore, e will be negative if SOTAB-II needs to turn starboard, and positive if it needs to turn port. TD' can be in the range of $-165° < TD' < 165°$ (i.e., Region I or Region II) (Figure 6.1 (A)). However, this design is problematic as higher TD' values may lead to rudder saturation and integral windup. To avoid this problem, TD' is

scaled down by a factor g in the PID control law. Therefore, the heading error can be defined as shown in Eq. 6.6. In order to anchor the robot's position to the oil slick within the maneuverable range of the rudder, a heading error input to rudder PID control law for tracking of a time-varying target heading was designed according to Eq. 6.7.

$$e = g * TD' - \theta \tag{6.6}$$

$$\delta(t) = e(t) + Kd\dot{e}(t) + K_i \int e(\tau)d\tau \tag{6.7}$$

Broadly speaking, the relative position of SOTAB-II with respect to the slick can be divided into three states: in mode or surrounded by oil (i.e., Case A,$\sum_{j=1}^{12} P_i(s_j) \geq 12$), out of slick (i.e., Case B $\sum_{j=1}^{12} P_i(s_j) = 0$) and edge mode (i.e., Case C, $\sum_{j=1}^{12} P_i(s_j) < 12$) Consequently, SOTAB-II autonomously maneuvers itself to move inside the slick if $\sum s_j < 12$, by not varying TD' in Eq. (6.6) during edge or out modes unless it has achieved the required maneuver.

6.2.3 Brake Board Control

In the case of the brake board, only two positions are selectable: off and on. Off denotes the condition for decreasing the drag force where the face of the brake board with the maximum surface area is oriented along the longitudinal direction of SOTAB-II. On denotes the condition for increasing the drag force where the face of the brake board is perpendicular to the longitudinal direction of SOTAB-II. Respective brake board orientation is determined based on the dynamic responses of SOTAB-II. The brake board, therefore, is positioned off when there is insufficient wind force to provide SOTAB-II with the thrust needed to catch the oil slick, or if it loses track of the oil slick and has to look for it again.

7 Pond Experimental Results

7.1 Experimental Results and Analysis

Various attempts were made to verify and optimize the control scheme. However, before testing the system in rough water, field experiments were performed in the Osaka University pond to ensure that the system is ready for open waters (Figure. 7.1 (A)). The field experiments were conducted to validate SOTAB-II's autonomous oil spill tracking capabilities and to test the guidance and navigation capability of SOTAB-II based on input from onboard sensors and control logic to derive target headings and directions. Three types of experiment were conducted to study the behavior of SOTAB-II, with each of these experiments described in detail below.

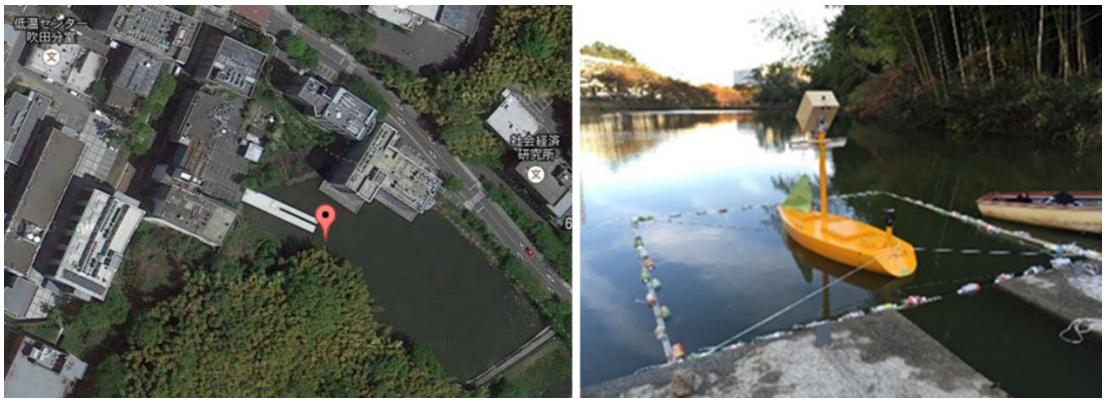

Figure 7.1 Experimental pond (Left) Experimental site, (Right) Floating fence to restrict the initial drift of SOTAB-II & Neoprene sheet

7.1.1 Free drift test

Free drifting experiments were performed to characterize the drifting behavior of the SOTAB-II. Throughout the experiment, the robot was allowed to drift with a fixed sail length and zero rudder. The behavior of the system was analyzed offline based on the saved sensor data. Figure 7.2 (top & bottom) shows the ratio of the buoy velocity to wind

velocity at 10m above sea level for free drifting with furled and unfurled sails. From Figure 7.2 (top & bottom), it can be concluded that SOTAB-II is capable of moving at 2–4.3% of wind speed with the available sail length.

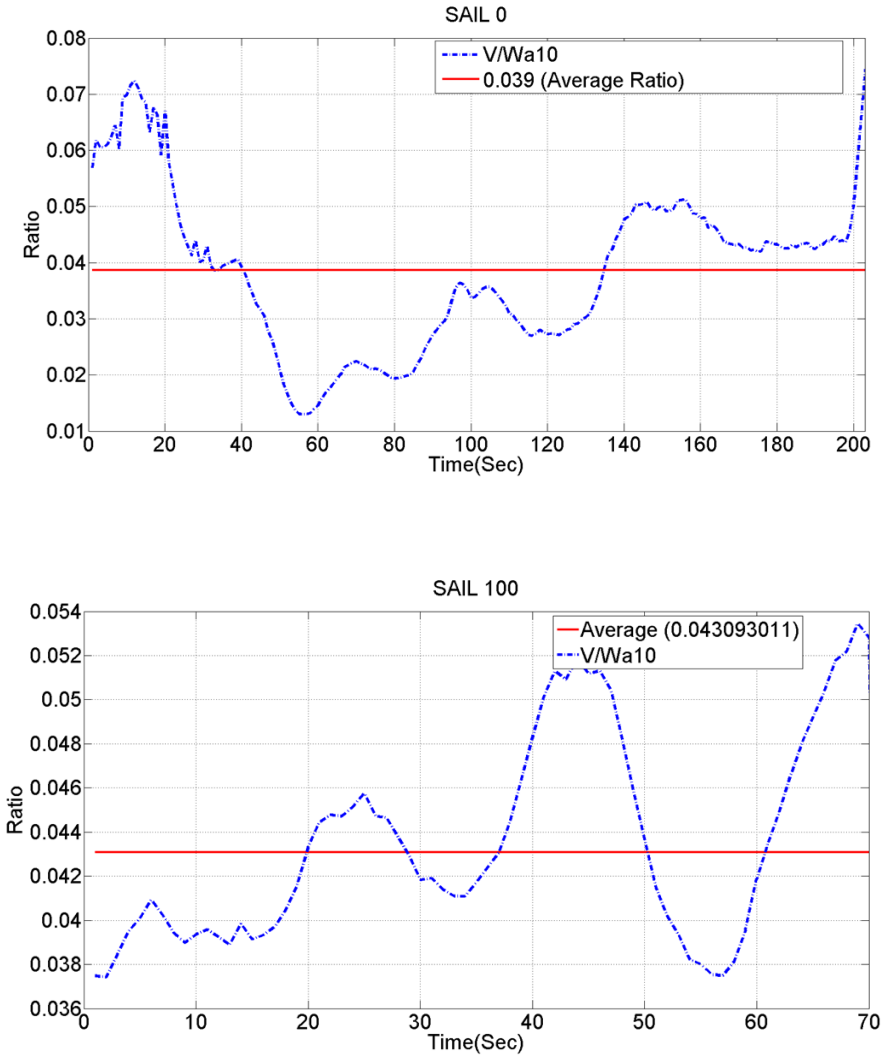

Figure 7.2 Ratio of buoy velocity to wind velocity at 10m above sea level (Top) with furled sail (Bottom) with unfurled sail

7.1.2 Heading Control & Speed Control Experimental Result

Subsequent speed control experiments were conducted on SOTAB-II using the sail and rudder. As previously mentioned, the drifting velocity of an oil spill is approximately 2.0–5.0% that of wind velocity in the direction of the wind at a height of 10m from the sea surface. Because the percentage of the wind velocity is not an exact value is yet to be confirmed or validated in our lab, as a matter of temporary expedience, we set a hypothetical wind velocity of 3.0% ($0.03 * \vec{W_a}$) at a height of 10m from the sea surface as the drifting velocity of an oil spill along the wind direction. In addition, this value ($0.03 * \vec{W_a}$) is the modified target speed ($TV' = 0.03 * \vec{W_a}$). Therefore, assuming the effect of water current on both spilled oil and SOTAB-II are the same, the goal of this experiment was test the steering of SOTAB-II along the wind while setting the sail to the optimal length in order to generate as much force as necessary to effectively move SOTAB-II with speed as deduced by TV'.

Figure 7.3(top) shows the time variation of TV', V, and sail length at each time interval. At $t = 50 - 60\ Sec, TV' < V$, we can see that in order to reduce the speed of SOTAB-II the sail length should be reduced. The same can be seen in Figure 7.3 (top), where sail length was found to decrease during the time interval mentioned above. In order to illustrate correlation between TV', V, and sail length in Figure 7.3 (top), the sail length magnitude has been scaled down; hence "1" denotes the unfurled sail and "0" denotes the furled sail. Therefore, it can be concluded that the sail is able to control SOTAB-II speed to move with desired TV'. Aiming to take full advantage of the wind effect under all conditions without generating lift-force in other directions, the sail direction was ruled perpendicular to the wind direction at all times. Hence, the modified target heading for this experiment was defined as $TD' = \beta$. Figure 7.3 (bottom) shows

the time variation of $\theta, e,$ and rudder response. Significant variations in e were controlled for because the oil sensor was not used in this experiment and $TD' = \beta$, hence g for this experiment was taken as "1" and e was updated at each interval. Therefore, it can be concluded that the rudder was effective in maneuvering SOTAB-II based on e. As buildings surround the experimental site, different streams of wind were experienced. Consequently, rudder was shown to be effective in controlling the heading direction of SOTAB-II within the desired limits.

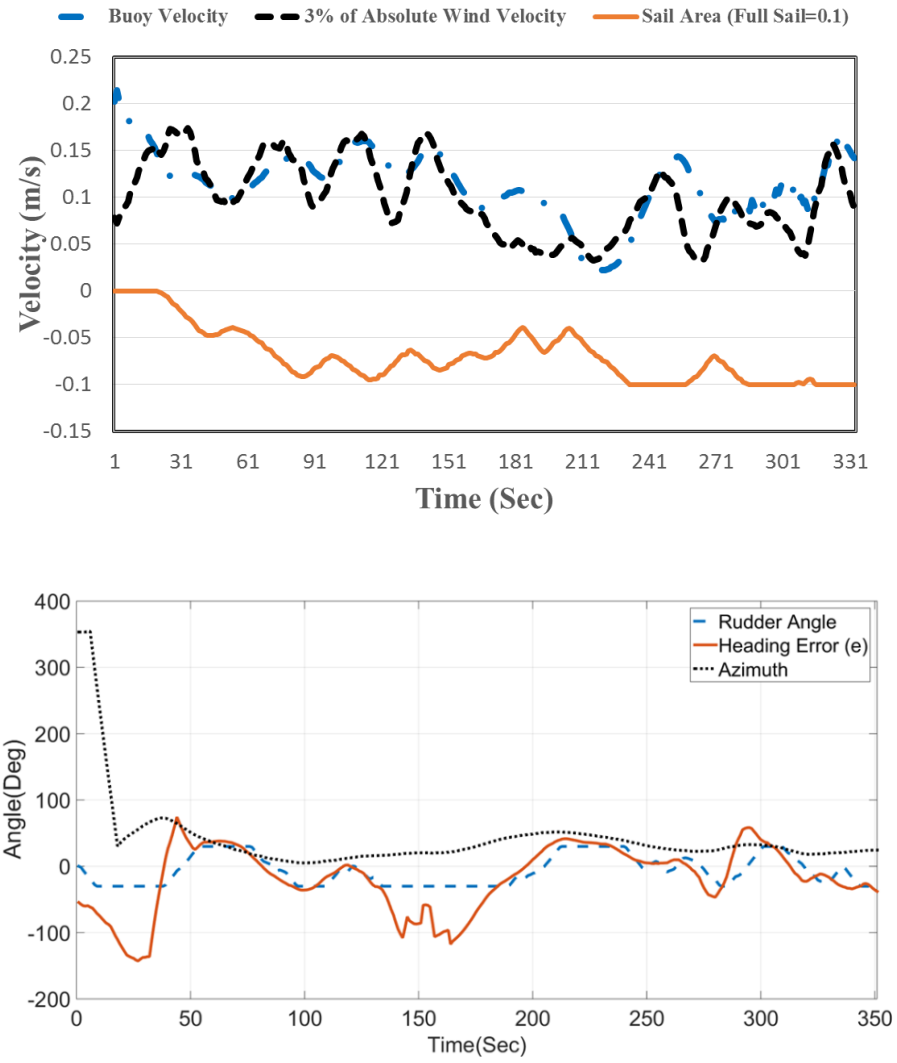

Figure 7.3 Behavior of SOTAB-II in pond (Top) SOTAB-II Speed control and sail response, (Bottom) SOTAB-II Heading control and rudder response

7.2 Simulated Oil Spill Tracking in Pond

As we were not permitted to use oil for testing the SOTAB-II control algorithm, we decided to build an artificial oil slick using neoprene sheets. Neoprene sheets were found to drift with a speed similar to that of CW_a and 3% of W_{a10}. Senga et al. (2013, 2009) and Yoshie et al. (2010) used 1 m × 1 m × 0.03 m square neoprene sheets for the original SOTAB-II experiments. From the experimental results, it was found that the edges of these neoprene sheet submerged in the water reducing the drift speed. Also, square sheets were found to rotate while drifting to achieve minimum drag, this phenomena made the sheets drift apart. To overcome this limitation, circular sheets were used for our experiment. Neoprene sponge rubber (0.10 m in diameter and 10 mm in thickness), pasted with white Sellotape, was used to simulate an oil spill in this experiment (Matsuzaki and Fujita 2013). This model of target was chosen because the oil sensor can give a false positive signal when focused on white fabric (Mahr and Chase 2008). A floating fence ($4 \times 4m^2$, Figure 7-1 (Right)) was used to restrict the initial drift of the neoprene sponge rubber and SOTAB-II. However, the neoprene sponge rubber was found to scatter and rapidly drift outside the detection zone of the oil sensor. Therefore, the control system was evaluated while the oil sensor could still detect them.

7.2.1 Pond Experiment Results for Tracking Largest Cluster of Simulated Oil Slick

Figure 7.4 (A) shows the time history of m_i (length of largest subarray), k_i (total number of largest subarray), and $\sum_{j=1}^{12} P_i(s_j)$ (sum of detected points in sensor data set at each time instant). We can see that at $t = 105$s, $\sum_{j=1}^{12} P_i(s_j) = 7, m_i = 3\ and\ k_i = 2$, this implies that there are two sequences of detected point of each length three. The starting indices of all the sequences have been shown in Figure 7.4 (B). From Figure 7.4 (B) we can see that the staring indices of two sequence of the largest subarray at $t = 105$, was found to be 0 and 9. This implies "Case C" needs to be followed for derivation of TD. Following the steps mentioned in "Case C" of perception, two Gaussian function with medians of 1.5 and 10, and a standard deviation of 3 were built. The probability of each target point belonging to the three clusters was decided based on Eq. (5.12–5.13). Figure 7.4 (C) shows the time history of cumulative sum of each cluster (product sum of Gaussian function and cumulative sum of sensor target point). From Figure 7.4 (C), we can confirm that cluster 1 will have the largest weighted sum among both clusters, which implies that the target heading will be the center of cluster 1 (i.e. $TD = -105°$). The same was reflected in the time history of TD (Figure 7.4 (D)).

Figure 7.4 (D) shows the time history of the target heading (TD), modified target heading (TD'), and relative wind direction ($-180° \leq \gamma \leq 180°$) at each instant of time. TD is calculated based on Eq. (5.13). As explained in the decision algorithm section "CASE C", the Gaussian based product sum of every cluster (i.e., $\max(sum_{ik})$) is compared with the previous Gaussian based product sum cluster sum (i.e.,$\max(sum_{(i-1)k})$), TD is decided based on the cluster having the largest sum value. This was done because there will be a higher probability of the buoy finding the neoprene

sheet if it goes in the direction of the cluster with the largest value. This was is shown in the time history of TD (Figure 7.4(C)). From Figure 7.4 (C) we can see that cluster with the largest sum was found around time $t = 98\ s$, at the same time instant $TD = -105$.

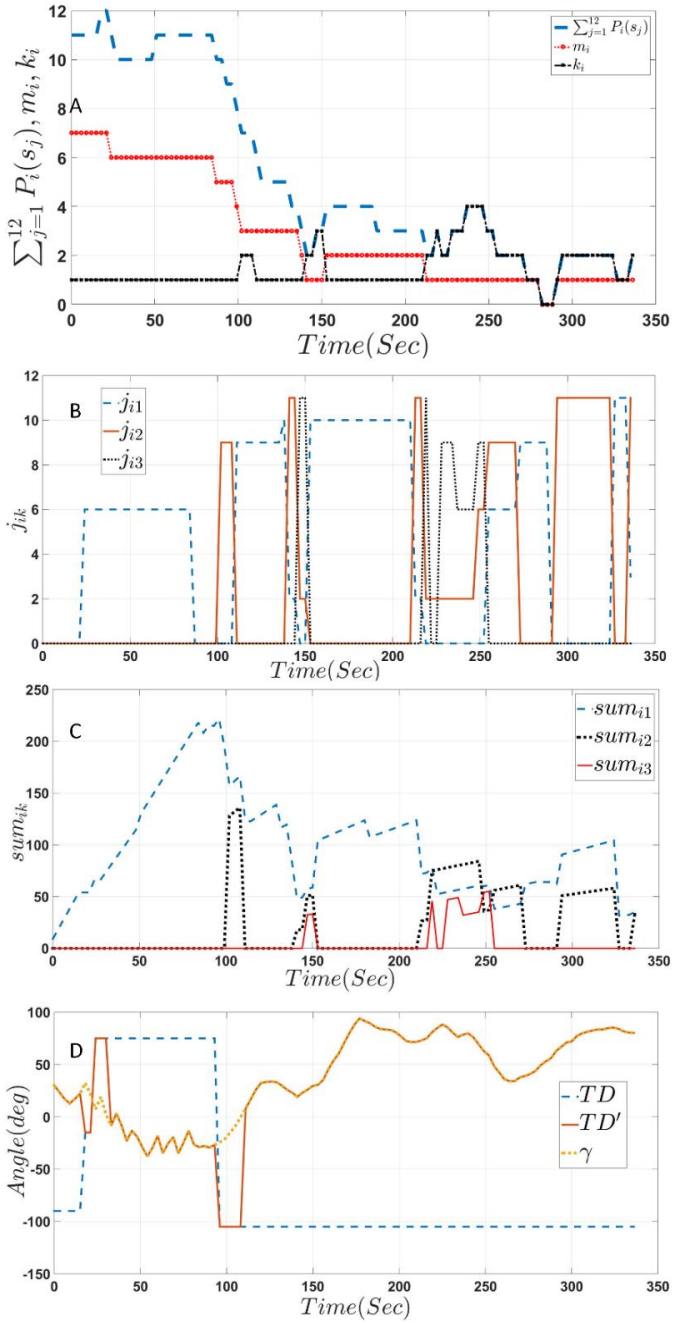

Figure 7.4 (A) Sensor data management in experiment (A) Total number of target points detected in each scan, length of largest subarray, total number of largest subarray in each sensor dataset; (B) Starting indices of each largest subarray in sensor data set (C) Gaussian Product Sum of each cluster, (D)T Time history variation of TD, TD' *, and* γ *at every time interval*

7.2.2 Pond Experiment Results for Tracking Largest Cluster of Simulated Oil Slick Discussion

Figure 7.5 shows extracts from the pond experiment video with their respective frame numbers. These pictures show the relative position of SOTAB-II with respect to the neoprene sheets at different time intervals. A Casio, EXILIM EX-100, operating at 29 frames per second, was used to video the experiment from a nearby rooftop. Frame 1500 in Figure 7.5 shows the starting condition of the experiment. SOTAB-II was tied using rope and a snap knot to the four corner of a fence that could be opened by just pulling the rope from a distance. At the start of the experiment, SOTAB-II found itself surrounded by the sheets, as shown in F1500 (Figure 7.5); while pulling the fence to allow SOTAB-II and the sheets to drift freely, a few sheets were found to be dragged by the fence and to form a cavity in the bow region of SOTAB-II (F3500, Figure 7.5). This phenomena lead to the formation of two neoprene sheet clusters surrounding SOTAB-II (Figure 7.4 (A) and Figure 7.5 (F4500 and F6000)). As explained in the decision-making algorithm, the cluster on the starboard side was found to have the greater Gaussian product sum (Figure 7.4(C), between 100 s and 110 s), and $\gamma < 0$, hence the navigation and control module commanded SOTAB-II to turn starboard, as can be seen in F4500 of Figure 7.5. Following this, the wind direction reversed ($TD \times \gamma < 0$), implying $TD' = \gamma$, this being reflected in the TD' time history (Figure 7.3 (D)). Following the navigational rule defined above, SOTAB-II tried to follow the neoprene sheet by moving downwind. As shown in Figure 7.5 (F10500), SOTAB-II was found at the end of the experiment to come to rest within a cluster of neoprene sheets and the largest cluster or patch of neoprene sheets was also found to be drifting in the same direction.

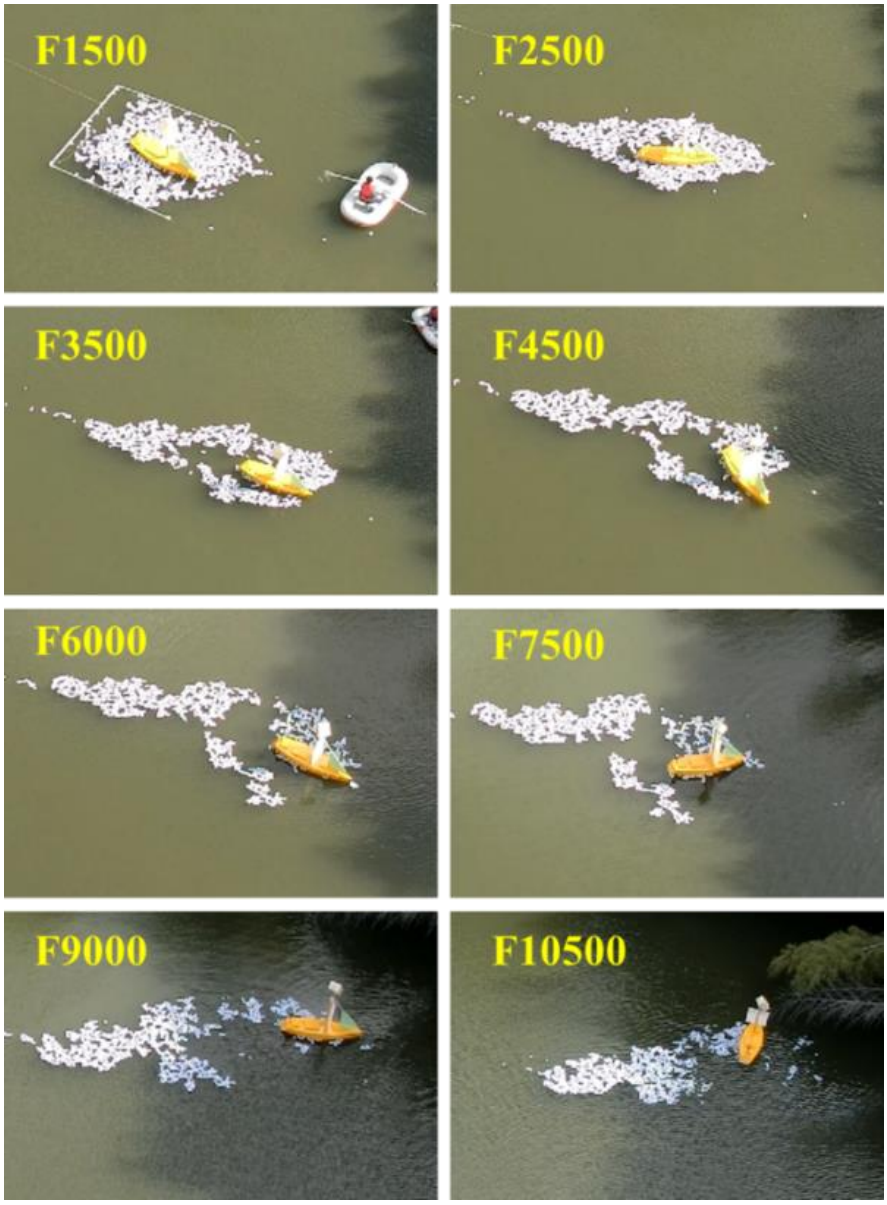

Figure 7.5 Pond experiment pictures with respective frame numbers

7.3 Pond Experiment Result & Discussion for Case B

Figure 7.6 shows extracted frames from the pond experiment video at different time instant with respective frame number. These pictures shows the relative position of SOTAB-II with respect to the neoprene sheets at different time instants. A Casio, EXILIM EX-100, operating at 29 frames per second, was used to video the experiment from a nearby rooftop. At the start of the experiment SOTAB-II was pulled out of the artificial

oil slick manually as shown in Fig. 7.6(F1000), Fig. 7.6(F3000) SOTAB-II starts tracking neoprene sheet based on line of sight algorithm as explained in CASE B. As estimated position of neoprene sheets lies towards the starboard side of SOTAB-II, Sotab-II can be seen taking starboard side turn (F6000-f13500). Finally SOTAB-II find neoprene sheets (Figure 7.6 (f13500)) and tries to get inside the neoprene sheet cluster. Figure 7.7 shows the estimated trajectory of the oil slick derived using oil sensor data, SOTAB-II trajectory, position of estimated oil slick and SOTAB-II, when SOTAB-II loses the track of oil slick and find it again. Figure 7.8(top) shows the time history of $\sum_{j=1}^{12}\sum_{i=1}^{n}P_i(s_j)$ at the time instant when SOTAB-II lost the simulated oil slick and when it detects again after losing the track of simulated oil slick. From Figure 7.8 (top) it can be seen that at $t = 73$ Sec, SOTAB-II loses the track of the simulated oil slick (Fig. 7.6(f3000)). At $t = 73$ Sec, the cumulative sum of $(\sum_{j=1}^{12}\sum_{i=1}^{n}P_i(s_j))$ of 180^0 (relative position of oil sensor in body coordinates) is largest, hence the estimated position of simulated oil slick will be SOTAB-II position when the oil sensor was scanning the target area at 180^0in body coordinates (Figure 6.1 (A)).

Same can be seen in Figure 7.7, estimated position of simulated oil slick lies behind the SOTAB-II absolute position (marked by black and yellow dots in Figure 7.7). Figure 7.8(bottom) shows the time history of TD , TD', γ and θ. From Figure 7.8(bottom) it can be seen that SOTAB-II tries to turn starboard side, but as the relative wind was blowing from starboard to port side it take some time for SOTAB-II to turn. SOTAB-II navigates as per decision and control algorithm and detects back the simulated oil slick around $t = 518$ Sec, same can be seen in Figure 7.6 (frame 13500), the cumulative sum target points shown an increment of one at target point of -150^0(Figure 10(top)), hence the estimated oil slick position should be at 3m away from the front of SOTAB-II (same can be seen in

the trajectory graph of SOTAB-II and simulated oil slick Figure 7.7).

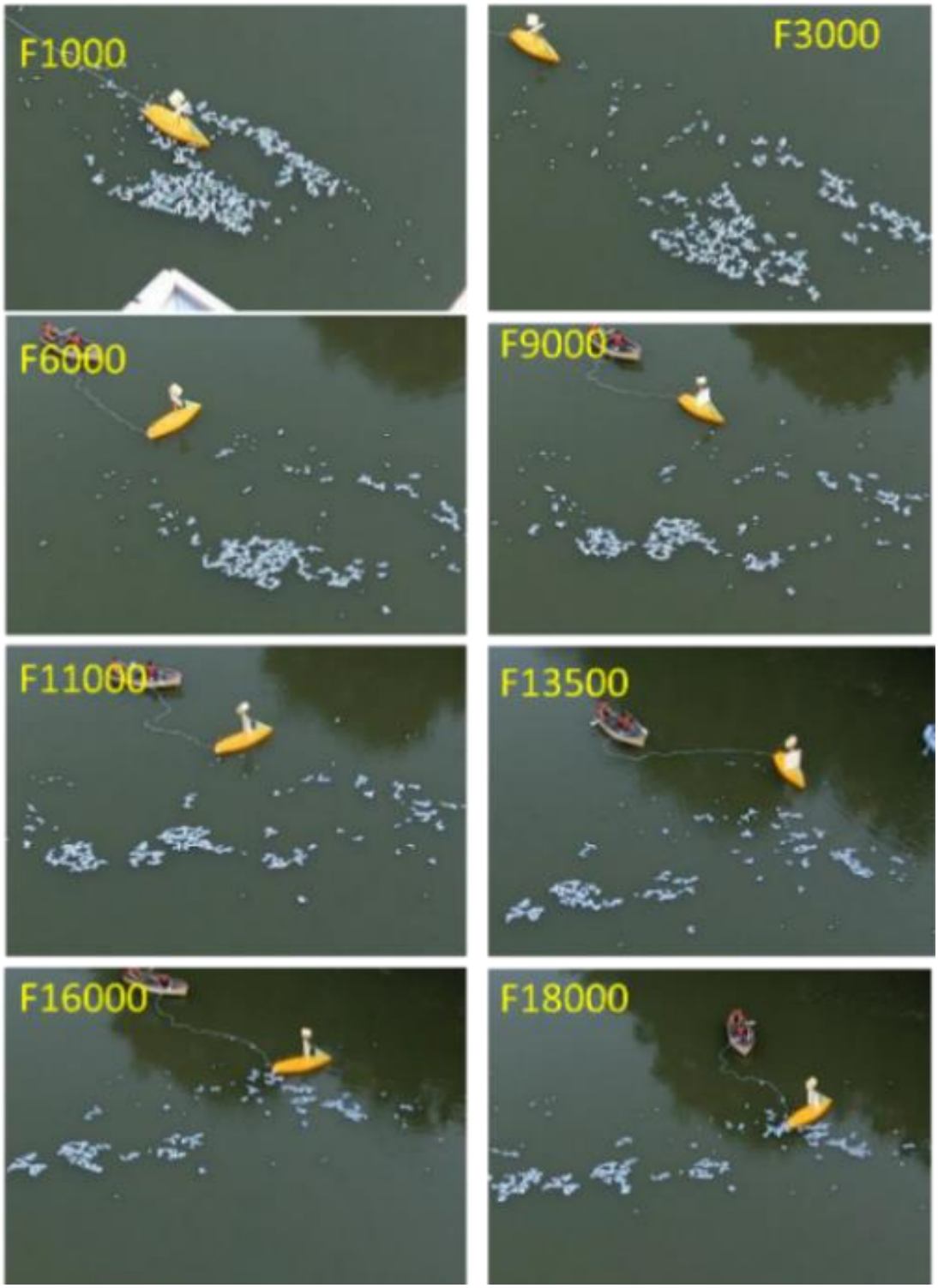

Figure 7.6 Pond experiment pictures at different time interval

From the Fig.7.6 it can be seen that SOTAB-II comes closer to few patches of simulated oil slick at various time instants (Figure 7.6 f9000), but as the oil sensor was scanning other target points at that time, hence cannot detect the patch near to it at that time. The decision algorithm keeps updating the TD and TD' , same has been reflected in Figure 7.8 (bottom). The decision making algorithm keeps projecting the estimated simulated oil slick position by distance travelled by virtual oil slick with a speed of TV , and direction given by $\psi\ i.e.$ absolute wind direction (Eq. 5. 5.5-5.6, as there are no water current in pond). From $t = 73$ to $t = 518Sec$ SOTAB-II did not find the simulated oil slick, hence the estimated oil slick position is given by (Eq. 5.8-5.9) second case. Hence, from the response behavior of SOTAB-II, it can be concluded that SOTAB-II control and decision algorithm is robust enough to bring back SOTAB-II within the slick autonomously without any human intervention in case it loses the track of the oil slick.

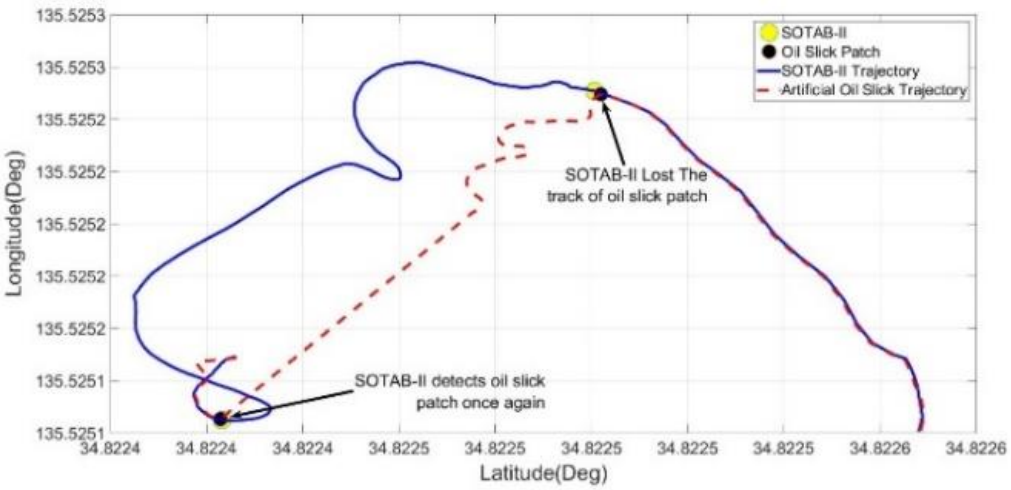

Figure 7.7 Estimated track of the oil slick & SOTAB-II trajectory

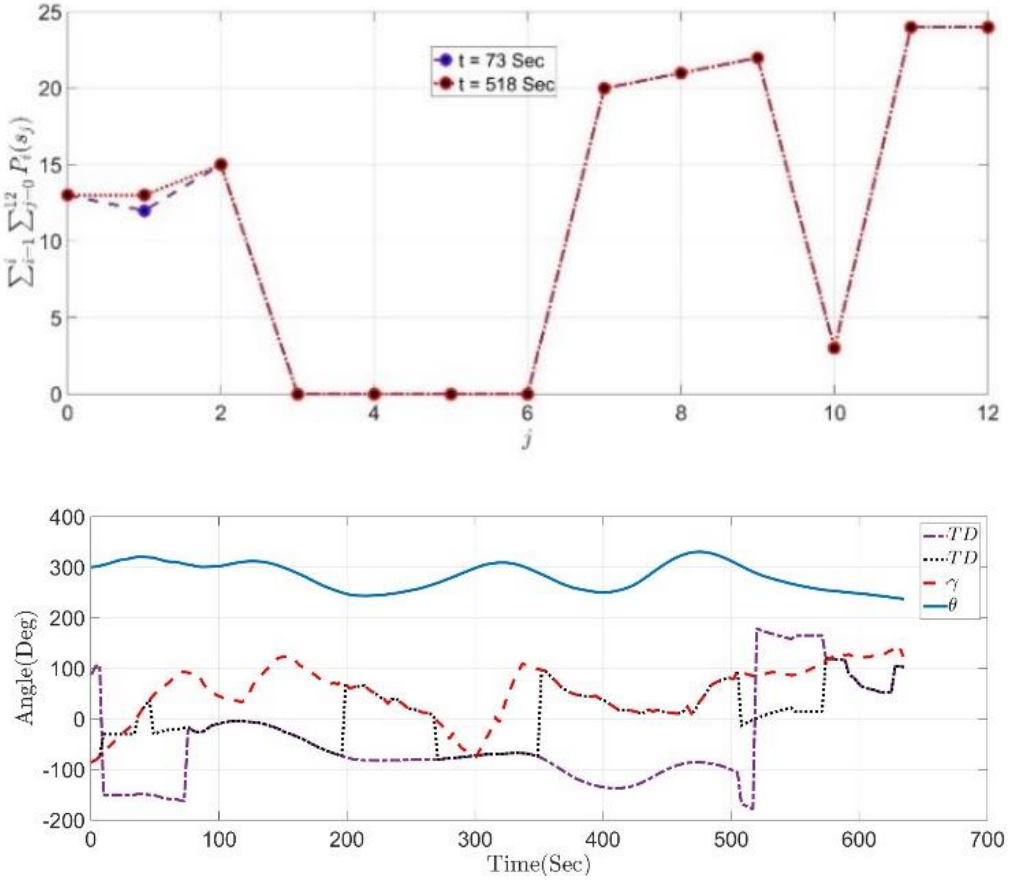

Figure 7.8 Time variations of parameters of guidance in experiment (Top) $\sum_{j=1}^{12}\sum_{i=1}^{n} P_i(s_j)$ *at* $t =$ 73 *and* $t = 518Sec$*, (bottom) Time history variation of* TD, TD' *,* γ *and* θ *at every time interval*

8 Sea Experiment Results

8.1 Free Drift Sea Test Results

Free drifting experiments were performed to characterize the drifting behavior of the SOTAB-II in the sea also. Throughout the experiment, the robot was allowed to drift with a fixed sail length and zero rudder. The behavior of the system was analyzed offline based on the saved sensor data. Table, II shows the ratio of the buoy velocity to wind velocity at 10m above sea level, for free drift with furled, semi unfurled, unfurled sail with brake board in turn-on condition, and for free drift with furled sail with brake board in turn-off condition. From Table II it can be seen that ratio of SOTAB-II speed and wind speed at 10m above sea level was found to increase by 1%, in case of free drift with furled sail and unfurled sail in brake board turn on condition. Similarly, ratio of SOTAB-II speed and wind speed at 10m height increased by 1%, while SOTAB-II drifting with furled sail and brake board in turn off condition to that of SOTAB-II drifting with semi unfurled sail and brake board in turn on condition.

Figure 8.1 Free drift experiment with unfurled sail

Table 8-1 Drift Speed Comparison

SAIL	BRAKE	$(V/W_{a10})\%$	W_{a10} (m/s)
0	90	2.57	7.44
50	90	3.53	4.99
100	90	4.03	6.81
0	0	4.61	4.88

Figure 8.2 shows the free drift trajectory of SOTAB-II with unfurled sail, water current, 3% of wind speed at 10m height and resultant of water current and 3% of wind speed at 10m height with free drift time of 239Sec. From the figure 8.2 it can be concluded that SOTAB-II is faster compared to resultant trajectory of water current and 3% of wind at 10m height.

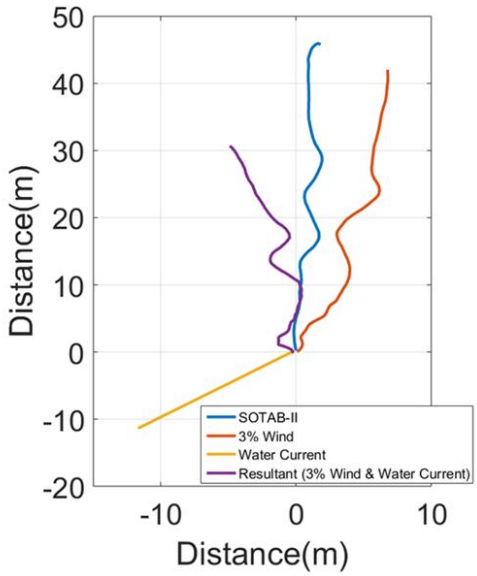

Figure 8.2 Free drift trajectory of SOTAB-II with unfurled sail, water Current, 3% wind and resultant of water current and 3% wind speed.

8.2 Sea Experiment Results for Tracking Largest Cluster of Simulated Oil Slick

From the results of the controlled drift experiment, it can be established that SOTAB-II drifts with water surface currents; therefore, in order to catch up with the simulate oil spill, the mainsail has to provide enough propulsive force to compensate for the wind induced drift. Following this assumption, the contribution of CW_a in all the equations mentioned above to formulate TD, TD', TV and TV' was neglected. This assumption was found to hold true in the experiments.

The same procedure as described previously for the pond experiment was carried out for sea experiment. Figure 8.3 shows extracts from the sea experiment video. These pictures show the relative position of SOTAB-II with respect to the neoprene sheets at different time intervals.

Figure 8.4 (A) shows the time history of m_i (length of largest subarray (i.e., oil slick patches surrounding SOTAB-II)), k_i (total number of large subarrays), and $\sum_{j=1}^{12} P_i(s_j)$ sum of detected points in sensor data set at each time interval. We can see that at $t = 313\ s, \sum P_i = 4, k = 4,$ and $m_i = 1,$ implying that there were four clusters of detected points, each of length one. The starting indices of all the sequences are shown in Figure 8.4 (B). From Figure 8.4 (B), we can see that the staring indices of all the four sequence of the largest subarray at $t = 313\ s$, was found to be 1, 4, 6, and 8. Hence, based on the Gaussian-based product sum algorithm, four Gaussian functions with centers of 1, 4, 6, and 8, and spread of 1, were defined. The probability of each target point belonging to the four oil slick patch groups was decided based on equations (5.16–5.17). Figure 8.4 (C) shows the time history sum_{ik} of each oil slick patch encountered while

tracking the oil slick. From Figure 8.4 (C), we can confirm that slick patch 1 was found to have the largest product sum among all the four slick patches, which implies that target heading will be the center of oil slick patch 1 (i.e., $TD = -150^o$). This can be seen in the time history of TD (Figure 8.4(D)).

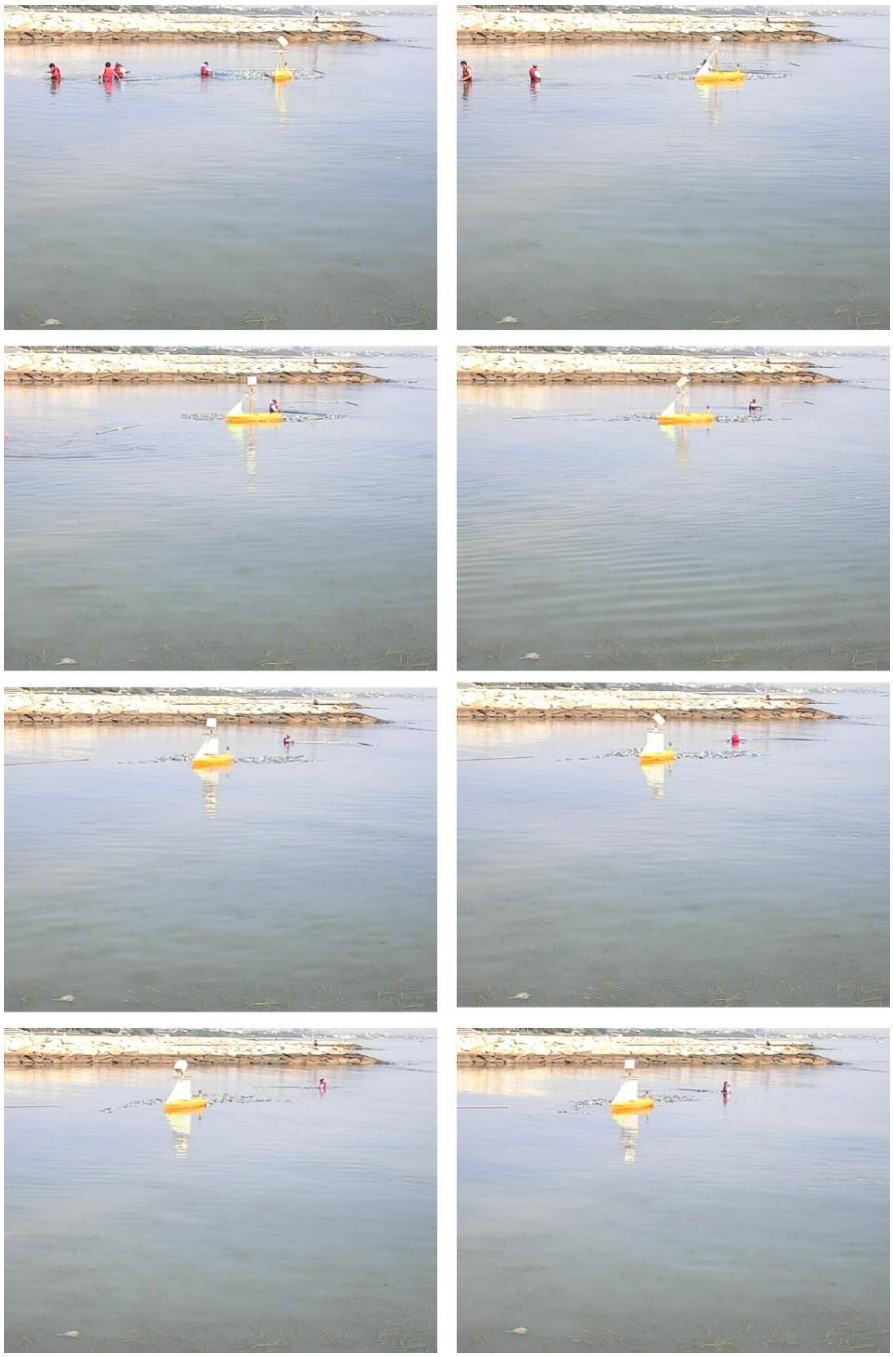

Figure 8.3 Sea experiment pictures at different time interval

Figure 8.4 (D), shows the time history of TD, TD' and γ at each time interval. TD is calculated based on Eq. (5.13). As explained above, the product sum of the Gaussian function dataset and the time history of cumulative sum of sensor data (i.e., $\max(sum_{ik})$) is compared at each time interval with the previous product sum (i.e., $\max(sum_{(i-1)k})$) and TD is determined based on the oil slick patch with the largest product sum value. This approach was taken because there is a higher probability of the buoy finding the neoprene sheets if it goes in the direction of the oil slick patch with largest product sum value. This was shown in the time history of TD (Figure 8.4 (D)). Comparing Figure 8.4 (C) and (D), it can be shown that the TD update rule (Equation 5.13) followed the time history variation of sum_{ik}.

Figure 8.5 shows the estimated trajectory of the simulated oil slick derived using oil sensor data, SOTAB-II trajectory, position of estimated oil slick, and estimated position of largest cluster and SOTAB-II when SOTAB-II loses the track of oil slick. Figure 8.4(c) shows the time history of the Gaussian product sum of each simulated oil slick cluster. From figure 8.4(A & C) it can be concluded that SOTAB-II encounters various small simulated oil slick patches, and the decision algorithm deduces the target heading and target speed to bring SOTAB-II closer to the largest cluster of the simulated oil slick patch. Figure 8.5 shows the absolute location of largest simulated oil slick cluster, simulated oil slick edge and SOTAB-II, based on this results it can be concluded that the decision algorithm is good enough in keeping SOTAB-II closer to the largest simulated oil slick patch.

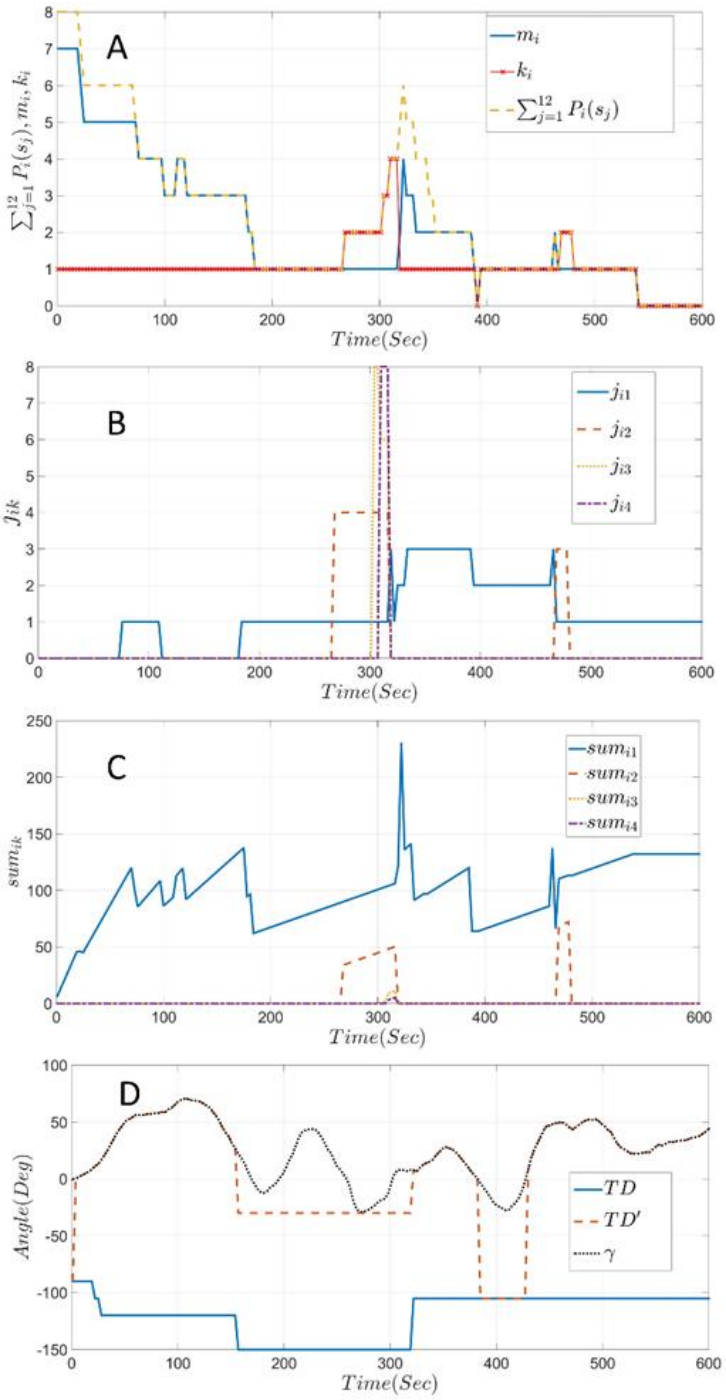

Figure 8.4 Data management for guidance and control at sea experiment (A) Total number of target points detected in each scan, length of largest subarray, total number of largest subarray in each sensor dataset; (B) Starting indices of each largest subarray in sensor dataset; (C) Gaussian product sum of each cluster; (D) Time history variation of TD,TD',and γ at every time interval.

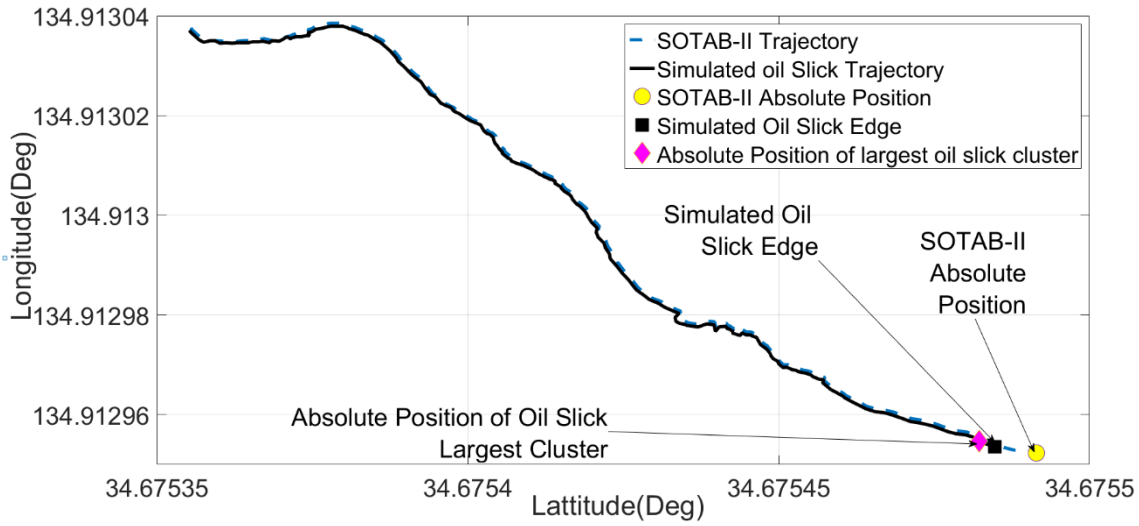

Figure 8.5 Estimated track of the oil slick & SOTAB-II trajectory

9 Conclusion & Future Work

9. 1 Conclusions

The new hull shape (KIT34) gives the independence of space requirements for batteries, motors, data acquisition and control electronics due to its broader beam and larger displacement compared to other sailing yachts of the same hull dimensions. In order to overcome the limitations of existing oil spill monitoring methods, SOTAB-II, equipped with a sail (the orientation and size of which are adjustable) and sensors to detect oil slicks on the sea surface, was developed. The use of laser fluorescence based oil sensor for oil detection reduce the probability of false signal.

The decision making algorithm considers time history of oil sensor data point to derive the target heading for guidance of SOTAB-II. This work has described a cluster-based path planning algorithm for the navigation of SOTAB-II. This clustering algorithm, based on the product sum of a Gaussian function and a time history of the cumulative sum of target points, reacts to the changing wind conditions, as well as the dynamic relative positioning of SOTAB-II, and simulated oil spills in real time. This method has been successfully tested in both a pond and moderate sea conditions. The sensor-based GNCS was validated through field experiments at the Osaka University pond and Eigashima Kobe beach; the results of which illustrate the free drifting velocity of SOTAB-II, its controlled drift via rudder and sail, and the ability of SOTAB-II to autonomous track simulated oil spills using an oil detection sensor.

The results of pond experiment illustrates that the free drifting velocity of SOTAB-II and its controlled drift via rudder and sail and the ability of SOTAB-II to autonomously track neoprene sheets, as an artificial oil slick, using an oil detection sensor. These pond

experiments have demonstrated that SOTAB-II is capable of moving at 2.0–4.3% of wind speed with furled and unfurled main sail and brake board in on condition (i.e. brake board is oriented in lateral direction). The sail and rudder are effective in controlling the speed of SOTAB-II within the desired range and controlling the heading direction within the desired limits. The pond experiments described in this work demonstrate that the trajectory of SOTAB-II was almost parallel to that of the cluster of neoprene sheets around SOTAB-II, suggesting that the GNCS functioned to follow the cluster of neoprene sheets as anticipated. Furthermore, the pond experiments described in this work demonstrate that the SOTAB-II was always found in close vicinity of the largest cluster of the simulated oil spill, suggesting that the GNCS functioned to follow the largest cluster of neoprene sheets as anticipated. Finally, the pond experiments described in this work demonstrate that the SOTAB-II was able to go back to simulated oil spill autonomously, suggesting that the GNCS upgraded with look ahead based algorithm functioned well to guide back SOTAB-II as anticipated.

Further sea experiments was carried out to validate the performance of SOTAB-II tracking artificial oil slicks in winds, waves, and currents at open sea. These experiments have demonstrated that SOTAB-II is capable of moving with a resultant velocity vector at 100% of water surface currents and at 2.5-5% of wind, and that the sail and rudder are effective in controlling the velocity of SOTAB-II within the desired range. Furthermore, the simulated oil spill tracking experiments described in this paper demonstrate that the SOTAB-II was following the largest of the neoprene sheet clusters surrounding the robot, suggesting that the GNC functioned to follow the largest simulated oil spill cluster as anticipated. This cluster-based algorithm can be easily adapted for multiple SOTAB-II deployments.

9.2 Future Work

A combination of mechanical recovery and non-mechanical technique such as in-situ burning and dispersant application forms the majority of the oil spill mitigation plan. The real time information of oil spill spread and oil spill thickness in both time and space are crucial to decide which mitigation plan to take. Hence, in order to estimate the spread of oil spill in real time multiple SOTAB-II will be needed. Multiple robots are frequently used for application such as surveillance and search operation. This has been possible due to the advance in recent technology and availability of inexpensive robots. However, coordination and formation of multiple robots in order to accomplish surveillance and search operation on large scale is still a challenge. Hence, multiple SOTAB-II control algorithm need to be developed to tackle colossal oil spill. The level of communication in between SOTAB-II's will plays a major role in multi SOTAB-II control.

The time history of oil sensor data available from the multiple SOTAB-II could be used to map the spread of oil spill. A data assimilation technique should be developed for using the variation of the time history of oil sensor data set in time and space with the oceanographic data (water current, wind and wave) for mapping the oil spill spread giving more insight into the patch formation of oil slick. This data assimilation can indirectly give the rough estimate of oil slick thickness.

10 References

Abril J, Salom J, Calvo O (1997) Fuzzy control of a sailboat. International Journal of Approximate Reasoning 16:359–375. doi:10.1016/S0888-613X(96)00132-6

Alves JC, Cruz NA (2008). FASt - an autonomous sailing platform for oceanographic missions. OCEANS 2008, Quebec City, September 2008. Institute of Electrical and Electronics Engineers, New York, pp 1–7. doi:10.1109/OCEANS.2008.5152114

Cruz NA, Alves JC (2008) Autonomous sailboats: An emerging technology for ocean sampling and surveillance. OCEANS 2008, Quebec City, September 2008. Institute of Electrical and Electronics Engineers, New York, pp 1–6. doi:10.1109/OCEANS.2008.5152113

Cruz NA, Alves JC (2010) Auto-heading controller for an autonomous sailboat. IEEE OCEANS – Sydney, Sydney, May 2010. Institute of Electrical and Electronics Engineers, New York, pp 1–6. doi:10.1109/OCEANSSYD.2010.5603882

Fay JA (1969). The spread of oil slicks on a calm sea. In: Hoult D, editor. Oil on the Sea. New York: Plenum Press. 53–64.

Fay JA (1971) Physical processes in the spread of oil on a water surface. Proc Joint Conf. Prevention Control of Oil Spills, Washington D.C: American Petroleum Institute. 653–663.

Fingas MF (1999). The evaporation of oil spills: development and implementation of new prediction methodology. Int Oil Spill Conf Proc, 1999 (1): 281–287.

Fingas M (2011) Buoys and devices for oil spill tracking. International Oil Spill Conference, Portland, May 2011. International Oil Spill Conference Proceedings, vol 20. International Oil Spill Conference Proceedings, Washington, p abs9. doi:10.7901/2169-3358-2011-1-9

Fingas M, Charles J (2001) The basics of oil spill cleanup, 2nd ed. Lewis Publishers, Boca Raton, Fla.

Fingas M, Brown CE (2007) Oil spill remote sensing: A forensic approach. In: Wang Z, Stout S (eds) Oil spill environmental forensics: Fingerprinting and source identification. Academic Press, Amsterdam, p 429–448

Fossen T. I (2002) Marine Control Systems: Guidance, Navigation and Control of Ships, Rigs and Underwater Vehicles. Marine Cybernetics.

Goodman R, Simecek-Beatty D, Hodgins D (1995) Tracking buoys for oil spills. International Oil Spill Conference, Long Beach, February–March 1995. International Oil Spill Conference Proceedings, vol 1. International Oil Spill Conference Proceedings, Washington, pp 3–8. doi:10.7901/2169-3358-1995-1-3

International Tanker Owners Pollution Federation [ITOPF] (2015) Statistics - ITOPF. http://www.itopf.com/knowledge-resources/data-statistics/statistics/. Accessed 19 Aug 2015

Ivichev I, Hole LR, Karlin L et al. (2012) Comparison of operational oil spill trajectory forecasts with surface drifter trajectories in the Barents Sea. Journal of Geology & Geosciences 1:1–8. doi:10.4172/2329-6755.1000105

JATEGAONKAR, R. V. Flight Vehicle System Identification: A Time Domain Methodology. Reston, VA: AIAA, 126. 2006.

Jensen H, Andersen J, Daling P et al. (2008) Recent experience from multiple remote sensing and monitoring to improve oil spill response operations. International Oil Spill Conference, Savannah, May 2008. International Oil Spill Conference Proceedings, vol 1. International Oil Spill Conference Proceedings, Washington, pp 407–412. doi:10.7901/2169-3358-2008-1-407

K. Nomoto. Analysis of kempf's standard maneuver test and proposed steering indices. Proceedings of 1st Symposium on Ship Maneuverability, 1960.

K. Nomoto, T. Taguchi, K. Honda, and S. Hirano. On the steering qualities of ships. International Shipbuilding Progress, Vol. 4, No. 35, 1957.

Kato N, Hiratsuka M, Senga H et al. (2010) Spilled oil tracking autonomous buoy. OCEANS 2010, Seattle, September 2010. Institute of Electrical and Electronics Engineers, New York, pp 1–9. doi:10.1109/OCEANS.2010.5664471

Kato N, Senga H, Suzuki H et al. (2012) Autonomous spilled oil and gas tracking buoy system and application to marine disaster prevention system. Interspill Conference, London, March 2012. Interspill, London.

Lekkas AM, Fossen TI (2012). A time-varying look ahead distance guidance law for path following maneuvering and control of marine craft. 9th IFAC Conference on Maneuvering and Control of Marine Craft, Riviera Ligure di Ponente, September 2012. International Federation for Automatic Control, Laxenburg, pp 398–403. doi:10.3182/20120919-3-IT-2046.00068

Mackay D, Leinonen PJ (1977) Mathematical model of the behaviour of oil spills on water with natural and chemical dispersion. Report EPS-3-EC-77–19. Environmental Protection Service, Fisheries and Environment Canada.

Mahr R, Chase CR (2009) Oil spill detection technology for early warning spill prevention. OCEANS 2009, Bremen, May 2009. Institute of Electrical and Electronics Engineers, New York, pp 1–8

Mariano AJ, Kourafalou VH, Srinivasan A, Kang H, Halliwell GR, et al. (2011) On the modeling of the 2010 Gulf of Mexico oil spill. Dyn Atmos Oceans 52(1):322–340.

Masuyama Y, Nakamura I, Tatano H et al. (1993) Dynamic performance of sailing cruiser by full-scale sea tests. 11th Chesapeake Sailing Yacht Symposium, Jersey City, January 1993. Society of Naval Architects and Marine Engineers, New York, pp 161–179

Masuyama Y, Fukasawa T (2011), “Tacking Simulation of SailingYachts with new Model of Aerodynamic Force Variation During Tacking Maneuver”, Journal of Sailboat Technology 2011-01.

Matsuzaki Y, Fujita I (2013) Horizontal turbulent diffusion at sea surface. Journal of Society of Civil Engineering & Coastal Engineering 69:460–480.

Morelli, E. A. and V. Klein. "Application of System Identification to Aircraft at NASA Langley Research Center." Journal of Aircraft, 42:1 (2005): 12-24

Petres C, Romero-Ramirez M, Plumet F et al. (2011) Modeling and reactive navigation of an autonomous sailboat. Proceedings of the 2011 IEEE/RSJ International Conference on Intelligent Robots and Systems (IROS), San Francisco, September 2011. Institute of Electrical and Electronics Engineers, New York, pp 3571 –3576

Plumet F, Petres C, Romero-Ramirez M et al. (2015). Toward an autonomous sailing boat. IEEE Journal of Oceanic Engineering 40:397–407. doi: 10.1109/joe.2014.2321714

Rathour SS, Akamatsu T, Kato N et al. (2014). Modelling and control design of spilled oil tracking autonomous buoy. 24th International Ocean and Polar Engineering Conference, Busan, June 2014. International Society of Ocean and Polar Engineers, Cupertino, pp 632–640

Rathour SS, Kato N, Tanabe N et al. (2015a) Spilled oil autonomous tracking using autonomous sea surface vehicle. Marine Technology Society Journal 49:102–116. doi: 10.4031/mtsj.49.3.15

Rathour SS, Kato N, Senga H et al. (2015b). Control algorithm for oil spill tracking using ASV with onboard oil detecting sensor. 25th International Ocean and Polar Engineering Conference, Kona, June 2015. International Society of Ocean and Polar Engineers, Cupertino, pp 645–652

Reed M, Johansen Q, Brandvik PJ, Daling P, Lewis A, et al. (1999) Oil spill modeling towards the close of the 20th century: overview of the state of the art. Spill Sci Technol Bull 5 (1): 3–16.

Ridder EJ, Vermeulen KJ, Keuning JA (2004). “A Mathematical Model for the Tacking Maneuver of a Sailing Yacht,” The International HISWA Symposium on Yacht design and Yacht Construction

Rynne P, von Ellenrieder K (2009) Unmanned Autonomous Sailing: Current status and future role in sustained ocean observations. Marine Technology Society Journal 43:21–30. doi:10.4031/mtsj.43.1.11

Senga H, Kato N, Ito A et al. (2009) Spilled oil tracking autonomous buoy system. Advanced Robotics 23:1103–1129. doi:10.1163/156855309x452476

Senga H, Kato N, Suzuki H et al. (2013) Field experiments and new design of a spilled oil tracking autonomous buoy. Journal of Marine Science and Technology 19:90–102. doi:10.1007/s00773-013-0233-2

Senga H, Kato N, Yu L et al. (2012) Verification experiments of sail control effects on tracking oil spill. OCEANS 2012, Yeosu, May 2012. Institute of Electrical and Electronics Engineers, New York, pp 1–7. doi:10.1109/OCEANS-Yeosu.2012.6263416

Stelzer R, Pröll T, John RI (2007) Fuzzy logic control system for autonomous sailboats. Proceedings of the IEEE International Fuzzy Systems Conference, London, July 2007. Institute of Electrical and Electronics Engineers, New York, pp 1–6. doi:10.1109/FUZZY.2007.4295347

Stelzer R, Pröll T (2008) Autonomous sailboat navigation for short course racing. Robotics and Autonomous Systems 56:604–614. doi:10.1016/j.robot.2007.10.004

Takagi Y, Ban T, Okano Y et al. (2012) Numerical tracking of methane gas/hydrate and oil droplet in deep water spill. 11th International Conference on Global Research and Education, Budapest, August 2012. Inter-Academia, Budapest, pp 1–8.

Tsutsukawa S, Suzuki Y, Kato N (2012) Efficacy evaluation of data assimilation for simulation method of spilled oil drifting. Proceedings of the 5th PAAMES and AMEC Conference, Taipei, December 2012. Pan Asian Association of Maritime Engineering Societies, Tokyo.

Unoki S (1993) Physical oceanography of the coast. Tokai University Press, Tokyo

Xiao L and Jouffroy J(2014). Modeling and nonlinear heading control of sailing yachts. IEEE Journal of Oceanic Engineering, 39(2):256–268.

Yamagishi S, Hitomi K, Yamanouchi H et al. (2000). Development and test of a compact lidar for detection of oil spills in water. Second International Asia-Pacific Symposium on Remote Sensing of the Atmosphere, Environment, and Space, Sendai, October 2000. International Society for Optics and Photonics, Sendai, pp 136–144.

Yoshie M, Kato N, Matsuzaki Y et al. (2010) A study on the autonomous buoy system tracking emulsified fuel oil on water through in-situ drifting experiment of the fundamental buoy system model and rubber sheets. Journal of the Japan Society of Naval Architects and Ocean Engineers 10:189–192.

Yoshie M, Matsuzaki Y, Fujit I et al. (2009) At-sea trial test of an autonomous buoy which tracks drifting oil and observation of in-situ data tracking drifting markers on the sea for predicting location of the spilled heavy oil. Proceedings of the 19th International Offshore and Polar Engineering Conference, Osaka, June 2009. International Society of Offshore and Polar Engineers, Mountain View, pp 437–444.

11 LIST OF PUBLICATION

Journal Papers

- Swarn Singh Rathour, N. Tanabae, N. Kato, H. Senga, Y. Hirai, M. Yoshie and T. Tanaka, "Spilled Oil Autonomous Tracking Using Autonomous Sea Surface Vehicle". *MTSJ, Volume 49, Number 3 – May/June 2015 Ocean Sensors for Ecosystems, Climate and Hazard Monitoring.*

Book Chapter

- Swarn Singh Rathour, N. Tanabae, N. Kato, H. Senga, M. Yoshie and T. Tanaka, "Development of a Robotic Floating Buoy for Autonomously Tracking Oil Slicks Drifting on the Sea Surface (SOTAB-II): Experimental Results". *Springer-Verlag, June 2016 Applications to Marine Disaster Prevention Spilled Oil and Gas Tracking Buoy System.*

Peer Reviewed Conferences

- Swarn Singh Rathour, T. Akamatsu, N. Kato, H. Senga, N. Tanabae, M. Yoshie, T. Tanaka, "Modelling and Control Design of Spilled Oil Tracking Autonomous Buoy". *Proceedings of the Twenty-fourth (2014) International Ocean and Polar Engineering Conference Busan, Korea, June 15-20, 2014*
- Swarn Singh Rathour, N. Tanabae, N. Kato, H. Senga, Y. Hirai, M. Yoshie and T. Tanaka, "Control Algorithm for Oil Spill tracking using ASV with on board Oil detecting Sensor". *Proceedings of the Twenty-fifth (2014) International Ocean and Polar Engineering Conference, USA, Kona, Big Island, Hawaii,, June 21-27, 2015*
- Swarn Singh Rathour, N. Tanabae, N. Kato, H. Senga, M. Yoshie and T. Tanaka, "An Autonomous Robotic platform for detecting, monitoring and tracking of oil spill on water surface". *OMAE - Conference on Ocean Offshore & Arctic Engineering, Busan, South Korea, JUNE 19-25, 2016.*

Symposium & National Conference

- Swarn Singh Rathour, N. Tanabae, N. Kato, H. Senga, M. Yoshie, T. Tanaka, "Sea Experiments on Autonomous tracking of Oil Spill using a Robotic Platform". *The 25th Ocean Engineering Symposium, Tokyo, Japan; 08/2015*

- Swarn Singh Rathour, N. Kato, H. Senga, N. Tanabae, M. Yoshie, T. Tanaka, "Experiments on Autonomous tracking of Oil Spill using a Robotic Platform". *Japan Society of Naval Architects and Ocean Engineers (JASNAOE Annual Autumn Meeting 2014)Japan, Nagasaki , November 20-21, 2014*
- Swarn Singh Rathour, N. Kato, Y. Chao, H. Senga, N. Tanabae, M. Yoshie, T. Tanaka, "Autonomous Sea Surface Vehicle for Oil Spill Tracking in Open Waters",. *32nd Annual Conference of Robotics Society of Japan, Japan, Fukuoka, September 4-6, 2014*